Comput. Methods Appl. Mech. Engrg. 274 (2014) 237–263

Contents lists available at ScienceDirect

Comput. Methods Appl. Mech. Engrg.

journal homepage: www.elsevier.com/locate/cma

Improving the *k-compressibility* of Hyper Reduced Order Models with moving sources: Applications to welding and phase change problems

Alejandro Cosimo [a], Alberto Cardona [a,*], Sergio Idelsohn [a,b,c]

[a] Centro de Investigación de Métodos Computacionales (CIMEC), Universidad Nacional del Litoral-CONICET, Güemes 3450, S3000GLN Santa Fe, Argentina
[b] Centro Internacional de Métodos Numéricos en Ingeniería (CIMNE), Barcelona, Spain
[c] Institució Catalana de Recerca i Estudis Avançats (ICREA), Barcelona, Spain

ARTICLE INFO

Article history:
Received 27 September 2013
Received in revised form 25 January 2014
Accepted 17 February 2014
Available online 3 March 2014

Keywords:
Reduced Order Models
Hyper reduction
Welding
Phase change
Moving sources
Proper Orthogonal Decomposition

ABSTRACT

The simulation of engineering problems is quite often a complex task that can be time consuming. In this context, the use of Hyper Reduced Order Models (HROMs) is a promising alternative for real-time simulations. In this work, we study the design of HROMs for non-linear problems with a moving source. Applications to nonlinear phase change problems with temperature dependent thermophysical properties are particularly considered; however, the techniques developed can be applied in other fields as well.

A basic assumption in the design of HROMs is that the quantities that will be hyper-reduced are *k-compressible* in a certain basis in the sense that these quantities have at most k non-zero significant entries when expressed in terms of that basis. To reach the computational speed required for a real-time application, k must be small. This work examines different strategies for addressing hyper-reduction of the nonlinear terms with the objective of obtaining *k-compressible* signals with a notably small k. To improve performance and robustness, it is proposed that the different contributing terms to the residual are separately hyper-reduced. Additionally, the use of moving reference frames is proposed to simulate and hyper-reduce cases that contain moving heat sources. Two application examples are presented: the solidification of a cube in which no heat source is present and the welding of a tube in which the problem posed by a moving heat source is analysed.

1. Introduction

Modelling problems that are intractable from the point of view of reaching real time computational speed are quite frequently found in science and in engineering. Two particularly time-consuming cases are the problems of welding and nonlinear phase change. This paper presents hyper-reduction methods for these two problems, but the methods developed can be extended to many other problems with similar characteristics.

A welding problem is essentially a thermally driven process. Due to this fact, a correct description of the heat source that represents the energy input is of great importance. Generally, this input is described in terms of a standardised and highly concentrated moving heat source. This feature sets up a problem whose main characteristics are rather rapid changes in the

* Corresponding author. Tel.: +54 3424511595x1013.
E-mail addresses: alecosimo@gmail.com (A. Cosimo), acardona@intec.unl.edu.ar (A. Cardona), sergio@cimne.upc.edu (S. Idelsohn).

http://dx.doi.org/10.1016/j.cma.2014.02.011
0045-7825/

involved fields as well as the rapid variation of material properties. The concentrated behaviour of the heat source introduces constraints in the size of the mesh and time step used to run the simulation, thus forcing an increment in the number of degrees of freedom of the problem.

Simulation of a welding problem is a highly complex task described as a Thermo-Mechanical-Metallurgical (TMM) process [1]. To reduce this complexity, certain simplifications are applied, such as describing the governing physics of the problem with a staggered thermo-mechanical model [2]. Despite efforts to render treatment of the problem more amenable, its complexity makes it unaffordable from the perspective of real-time simulations. In this context, the design of Reduced Order Models (ROMs) is an elegant and promising alternative to the classical high fidelity solutions.

Currently, the use of separate representations to build ROMs has caught the attention of the engineering community. The manner in which the separated representation is built is described by two approaches [3]. In one approach, *a posteriori* model reduction techniques require knowledge of the solution to a training problem. The most prominent *a posteriori* technique is based on the Proper Orthogonal Decomposition (POD) method [4,5]. For the second approach, the *a priori* model reduction techniques require no previous knowledge of the solution, concept which was introduced by Ryckelynck in [6]. In this context, the leading technique is the Proper Generalised Decomposition (PGD), which has its roots in the works of Ladevèze [7,8].

In both approaches, to successfully address the high dimensionality of the problem, it is assumed that the solution can be described in terms of a reduced number of functions in the separate representation. In a certain sense, this situation can be referred to as the *separate representation hypothesis*. A consequence of this idea is the supposition that the solution of the problem is *k-compressible* in a certain basis, with a notably small k. The solution is said to be *k-compressible* if it has at most k non-zero significant entries when expressed in terms of that *magic* basis. An extensive analysis of similar concepts is offered in the context of compressed sensing, see, for example [9,10].

The present work considers the *a posteriori* ROM technique based on the POD method. The reduction of the problem begins by reducing the dimensionality of the discrete versions of the test and trial spaces. This process is generally carried out by finding a basis, say $\boldsymbol{\Theta}$, in which the solution to the problem is *k-compressible*, which is obtained by computing the Singular Value Decomposition of a set of snapshots of the solution. Next, the trial solution space is defined as an affine translation of $span\{\boldsymbol{\Theta}\}$. If a Bubnov–Galerkin projection is used, the test functions are in $span\{\boldsymbol{\Theta}\}$. It must be mentioned that a Petrov–Galerkin projection is recommended for problems where the Jacobian is not symmetric positive definite (SPD), which involves the solution of a least squares problem [11].

After reducing the dimensionality of the test and trial spaces, the size of the system of linear equations to be solved is reduced from a size of $N \times N$, where N is the size of the high fidelity (HF) model, to a size of $k \times k$, with $k \ll N$. With this approach, although the computational cost of solving the system of linear equations is reduced, the cost of assembling the residual and the tangent matrix at each Newton iteration is still of order N. It is widely known that to significantly reduce the computational complexity of the problem, the cost of assembling the residual and the tangent matrix at each Newton iteration must be reduced [11–16]. To accomplish this objective, a second reduction is performed by evaluating the involved quantities at a few points of the domain. Extensions of this idea have been used in the context of *a priori* and *a posteriori* reduction methodologies. For instance, in [17] the extension to nonlinear Finite Element models making use of an *a priori* approach is presented and the term hyper-reduction is coined to refer to the general procedure of performing a second reduction. Another work following this line is that of Sarbandi et al. [18].

In the context of *a posteriori* reduction techniques, the hyper-reduction method has been widely applied. Generally, the ideas along this path are based on the gappy data reconstruction method introduced by Everson and Sirovich [19] in the image processing community. For example, an extension of this idea to Finite Volume equations was accomplished by Astrid [20], extensions to nonlinear mechanical models are found in [13,21] and, in the case of computational fluid dynamics, treatments of this kind are found in [14,15]. In the present work, we use the term Hyper-Reduced Order Models (HROMs) to refer to the reduced models arising from the hyper-reduction method. To the authors' best knowledge, the design and application of HROMs specifically suited for phase change and welding problems have not yet been addressed in the literature.

In this paper, different approaches are studied in detail for the design of HROMs with particular application to the nonlinear phase change problem. Schemes in which the residual is hyper-reduced as a unit, taking the history of the residual as snapshots for the gappy data reconstruction procedure, are usually found in the literature [11,14]. This strategy is used as a reference technique for comparison in this work. As observed from numerical experiments, poor *k-compressibility* and tangent matrix conditioning are obtained when applying this technique for the design of HROMs. To improve the performance and robustness, it is proposed that the different contributing terms to the residual are separately hyper-reduced. These terms are assumed to be physically based nonlinear generalised contributing forces, features that lead to a well-posed HROM. In the case of welding problems, the moving heat source represents an issue that can severely affect the *k-compressibility* of the involved terms. This complication is addressed by considering both moving and fixed frames of reference respect to the welded piece.

The paper is organised as follows. Section 2 states the mathematical formulation of the solid–liquid phase change problem, and Section 3 presents the formulation of Reduced Order Models. The cost of assembling the nonlinear forces and tangent matrices is reduced by means of Hyper Reduced Order Models in Section 4, significantly reducing the computational complexity of the problem. In Section 5, the issue presented by the moving heat source is considered, and two application examples are presented in Section 6 to assess the performance of the introduced HROMs. Specifically, the solidification of a cube and welding of a tube without material deposition are analysed. Finally, Section 7 describes the main conclusions of this work.

2. Problem setting

The physical problem under consideration is a nonlinear transient heat conduction problem in which the liquid–solid phase change and thermophysical properties that depend on temperature are taken into account. Assuming that the contribution of the mechanical energy to the total energy is negligible and considering the specific enthalpy $\mathcal{H}$ as a thermodynamic potential, the temperature field T is computed by solving the heat balance equation

$$\rho\dot{\mathcal{H}} = Q + \nabla\cdot(k\nabla T) \quad \forall(\boldsymbol{x},t)\in\Omega_i\times(t_0,\infty), \tag{1}$$

where ρ is the density, k is the thermal conductivity, T is the temperature, Q is the external heat source per unit volume, and Ω_i for $i\in[s,l]$ are the solid and liquid sub-domains with $\Omega_s\cap\Omega_l=\{\emptyset\}$ and $\Omega=\Omega_s\cup\Omega_l$. The temperature field should verify the initial conditions

$$T = T_0 \quad \forall\boldsymbol{x}\in\Omega,\ t=t_0, \tag{2}$$

where $T_0(\boldsymbol{x})$ is the given initial temperature field. Additionally, the following set of conditions must be verified at the disjoint portions $\Gamma_d,\ \Gamma_q,\ \Gamma_c$ of the external boundary

$$T = T_d \quad \forall(\boldsymbol{x},t)\in\Gamma_d\times(t_0,\infty), \tag{3}$$
$$k\nabla T\cdot\boldsymbol{n} = q_w \quad \forall(\boldsymbol{x},t)\in\Gamma_q\times(t_0,\infty), \tag{4}$$
$$k\nabla T\cdot\boldsymbol{n} = h_f(T_f - T) \quad \forall(\boldsymbol{x},t)\in\Gamma_c\times(t_0,\infty), \tag{5}$$

where $\Gamma_d\cup\Gamma_q\cup\Gamma_c=\partial\Omega,\ T_d$ is the imposed temperature at the boundary $\Gamma_d,\ q_w$ is the external heat flow at the boundary $\Gamma_q,\ h_f$ is the heat convection coefficient, T_f is the external fluid temperature at the portion the boundary Γ_c and $\boldsymbol{n}$ is the outward normal to the boundary under consideration. Finally, at the interface Γ between Ω_s and Ω_l (the phase change boundary), the following constraints must hold

$$T = T_m \quad \forall(\boldsymbol{x},t)\in\Gamma\times(t_0,\infty), \tag{6}$$
$$[-(k\nabla T)\cdot\boldsymbol{n}_\Gamma]_\Gamma = \rho\mathcal{L}u_\Gamma \quad \forall(\boldsymbol{x},t)\in\Gamma\times(t_0,\infty). \tag{7}$$

In these equations, $\mathcal{L}$ is the latent heat, T_m is the melting temperature, $\boldsymbol{n}_\Gamma$ is the outward normal to the solidification front from the solid domain, $u_\Gamma=\boldsymbol{u}_\Gamma\cdot\boldsymbol{n}_\Gamma$ is the velocity of the interface in the direction of the normal $\boldsymbol{n}_\Gamma$ and the operator $[\bullet]_\Gamma$ measures the jump of the quantity $\bullet$ at the solidification front. Eq. (6) imposes the constraint that the temperature at the phase change boundary must be equal to the melting temperature and Eq. (7) is the interface condition (the Stefan condition).

The specific enthalpy $\mathcal{H}$ can be expressed in terms of the temperature T as

$$\mathcal{H}(T) = \int_{T_{\text{ref}}}^{T} c(\tau)d\tau + \mathcal{L}f_l(T), \tag{8}$$

where T_{ref} is a reference temperature, $c(\tau)\equiv c$ is the heat capacity and $f_l(T)$ is the liquid fraction. For an isothermal phase change, the liquid fraction is expressed as a Heaviside step, i.e., $f_l = H_{eav}(T-T_m)$. In the case of non-isothermal phase change, the liquid fraction can be described in terms of a linear function of temperature with solidus temperature T_{sol} and liquidus temperature T_{liq} as parameters and given by

$$f_l(T) = \begin{cases} 1 & \text{if } T > T_{liq}, \\ \frac{T-T_{sol}}{T_{liq}-T_{sol}} & \text{if } T_{sol}\leqslant T\leqslant T_{liq}, \\ 0 & \text{if } T < T_{sol}. \end{cases} \tag{9}$$

The energy input to the medium is described in terms of the Goldak heat source [22], given by

$$Q(\boldsymbol{\xi}(\boldsymbol{x}),t) = \frac{6\sqrt{3}Q_s}{\pi\sqrt{\pi}bc}\begin{cases} \frac{f_f}{a_f}\exp\left(-3\frac{\boldsymbol{\xi}\cdot\boldsymbol{\xi}}{\boldsymbol{a}_f\cdot\boldsymbol{a}_f}\right) & \text{if } \xi>0, \\ \frac{f_r}{a_r}\exp\left(-3\frac{\boldsymbol{\xi}\cdot\boldsymbol{\xi}}{\boldsymbol{a}_r\cdot\boldsymbol{a}_r}\right) & \text{if } \xi\leqslant 0, \end{cases} \tag{10}$$

where $\boldsymbol{a}_f=[a_f,b,c],\ \boldsymbol{a}_r=[a_r,b,c],\ \boldsymbol{\xi}=[\xi,\eta,\gamma],\ a_f$ and a_r are the length parameters associated with the axis of the front and rear semi-ellipsoids, respectively; b and c are the other axes of the semi-ellipsoids; f_f and f_r are the portion of heat distributed in the front and rear semi-ellipsoids, such that $f_f+f_r=2;\ t$ is the time and Q_s is the total heat input. Generally, Q_s is specified in terms of the electric current I, the voltage V and the heat source efficiency η, as $Q_s=\eta IV$. The local coordinate system $\boldsymbol{\xi}$ is attached to the heat source as shown in Fig. 1.

2.1. Variational formulation and finite element discretisation

The variational formulation of the problem and its finite element discretisation is briefly described in this section. Further details can be found in references [23,24]. Let $\mathcal{S}=\{T/T\in\mathcal{H}^1(\Omega),\ T|_{\Gamma_d}=T_d\}$ be the space of trial solutions and

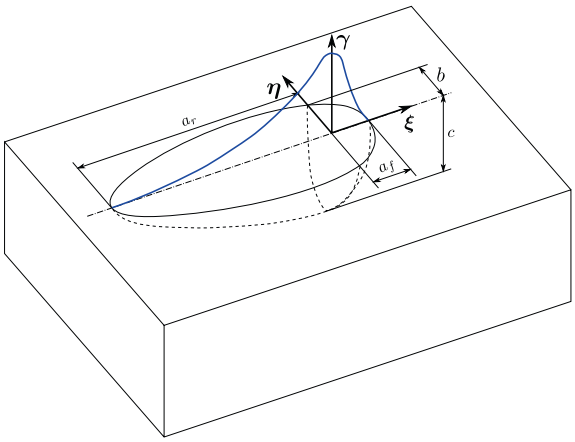

Fig. 1. Goldak heat source.

$\mathcal{V} = \{v / v \in \mathcal{H}^1(\Omega),\ v|_{\Gamma_d} = 0\}$ be the space of weighting or test functions, where $\mathcal{H}^1$ is the first order Sobolev space. Next, the variational formulation is given as follows:

Find $T \in \mathcal{S}$ *such that* $\forall w \in \mathcal{V}$

$$\int_\Omega w\left[\rho c\frac{\partial T}{\partial t} + \rho\mathcal{L}\frac{\partial f_l}{\partial t} - Q\right] d\Omega + \int_\Omega \nabla w \cdot (k\nabla T)\, d\Omega + \int_{\Gamma_c} w h_f (T - T_f)\, d\Gamma + \int_{\Gamma_q} w q_w\, d\Gamma = 0, \quad \text{for } t > 0;$$

$$\int_\Omega wT\, d\Omega = \int_\Omega wT_0\, d\Omega, \quad \text{for } t = 0. \tag{11}$$

We remark that in the case of isothermal phase change, the time derivative of the liquid fraction $\frac{\partial f_l}{\partial t}$ should be interpreted in a distributional sense.

Let $\mathcal{S}^h \subset \mathcal{S}$ and $\mathcal{V}^h \subset \mathcal{V}$ be subspaces of the trial and test functional spaces, respectively. Therefore, in matrix notation, $T^h \in \mathcal{V}^h$ is given by

$$T^h(\boldsymbol{x}, t_n) = \boldsymbol{N}^T \boldsymbol{T}_n, \tag{12}$$

where $\boldsymbol{N}$ denotes the finite element basis, such that $\mathbb{R}^N \in span\{\boldsymbol{N}\}$, and $\boldsymbol{T}_n \in \mathbb{R}^N$ denotes the FEM (Finite Element Method) nodal degrees of freedom, with N as the dimension of the FEM space. Linear shape functions are used in this work. Next, using a Bubnov–Galerkin projection and a Backward-Euler scheme for time integration, the discrete form of the residual of the nonlinear thermal problem reads

$$\boldsymbol{\Pi}_n = \boldsymbol{\Pi}(\boldsymbol{T}_n, t_n) = \boldsymbol{G}_n^c + \boldsymbol{G}_n^k + \boldsymbol{G}_n^l + \boldsymbol{F}_n - \boldsymbol{Q}_n = \boldsymbol{0}, \tag{13}$$

where

$$\boldsymbol{G}_n^c = \boldsymbol{G}^c(\boldsymbol{T}_n, t_n) = \int_\Omega \rho_n c_n \boldsymbol{N}\boldsymbol{N}^T\, d\Omega\ \frac{\boldsymbol{T}_n - \boldsymbol{T}_{n-1}}{\Delta t} \simeq \frac{\boldsymbol{H}_n^c - \boldsymbol{H}_{n-1}^c}{\Delta t}, \tag{14}$$

$$\boldsymbol{G}_n^k = \boldsymbol{G}^k(\boldsymbol{T}_n, t_n) = \left(\int_\Omega \nabla\boldsymbol{N} k_n \nabla\boldsymbol{N}^T \Omega + \int_{\Gamma_c} h_{f_n}\boldsymbol{N}\boldsymbol{N}^T\, d\Gamma\right)\boldsymbol{T}_n, \tag{15}$$

$$\boldsymbol{G}_n^l = \boldsymbol{G}^l(\boldsymbol{T}_n, t_n) = \frac{1}{\Delta t}\left(\int_\Omega \rho_n \mathcal{L}\boldsymbol{N} f_{l(n)}\ d\Omega - \int_\Omega \rho_n \mathcal{L}\boldsymbol{N} f_{l(n-1)}\ d\Omega\right) \simeq \frac{\boldsymbol{H}_n^l - \boldsymbol{H}_{n-1}^l}{\Delta t}, \tag{16}$$

$$\boldsymbol{F}_n = \boldsymbol{F}(t_n) = \int_{\Gamma_q} \boldsymbol{N} q_{w_n}\, d\Gamma - \int_{\Gamma_c} h_{f_n}\boldsymbol{N} T_{f_n}\, d\Gamma, \tag{17}$$

$$\boldsymbol{Q}_n = \boldsymbol{Q}(t_n) = \int_\Omega \boldsymbol{N} Q_n\, d\Omega. \tag{18}$$

Terms $\boldsymbol{G}_n^c$ and $\boldsymbol{G}_n^l$, which involve discrete time derivatives and represent generalised capacitance and latent heat forces in response to temperature increments, are approximated as generalised forces increments during the time step, Eqs. (14) and (16), where:

$$\boldsymbol{H}_n^c = \int_\Omega \rho_n c_n \boldsymbol{N}\boldsymbol{N}^T \, d\Omega \, \boldsymbol{T}_n, \tag{19}$$

$$\boldsymbol{H}_n^l = \int_\Omega \rho_n \mathcal{L}\boldsymbol{N} f_{l(n)} \, d\Omega. \tag{20}$$

Eq. (13) is therefore rewritten giving

$$\boldsymbol{\Pi}_n = \boldsymbol{\Pi}(\boldsymbol{T}_n, t_n) = \frac{\boldsymbol{H}_n^c - \boldsymbol{H}_{n-1}^c}{\Delta t} + \boldsymbol{G}_n^k + \frac{\boldsymbol{H}_n^l - \boldsymbol{H}_{n-1}^l}{\Delta t} + \boldsymbol{F}_n - \boldsymbol{Q}_n = 0. \tag{21}$$

In what follows the discussion will be directed towards obtaining highly *compressible* signals in the adopted formulation. This modification of the formulation will be advantageous in developing HROMs, for reasons that will be given in detail in Section 4.2.

It must be noted that $\boldsymbol{G}_n^l = \left(\boldsymbol{H}_n^l - \boldsymbol{H}_{n-1}^l\right)/\Delta t$ only when ρ does not depend on temperature. Also, note that in the nonlinear case $\boldsymbol{G}_n^c$ is different from $(\boldsymbol{H}_n^c - \boldsymbol{H}_{n-1}^c)/\Delta t$. Nevertheless, we assume that these approximations do not affect the accuracy. Take into account that the only differences are due to the fact that in the expressions $\boldsymbol{H}_{n-1}^l$ and $\boldsymbol{H}_{n-1}^c$, the material properties (ρ, c) are evaluated in terms of $\boldsymbol{T}_{n-1}$ instead of $\boldsymbol{T}_n$, a valid approximation for small time increments.

3. Formulation of the Reduced Order Model

The application of spatio-temporal separated representations for the formulation and design of the Reduced Order Model is studied next (for a general treatment of separated representations, see for instance [25]). In our case, to describe the unknown temperature $T(\boldsymbol{x}, t)$, we use the separated representation given by

$$T^h(\boldsymbol{x}, t) \simeq \sum_{j=1}^{M} S_j(\boldsymbol{x}) R_j(t) + T_d(\boldsymbol{x}, t), \tag{22}$$

where T_d denotes the non-homogeneous essential boundary conditions.

Both approaches, the *a posteriori* and *a priori* ROM techniques, make use of this idea. These methods assume that the response of the system under study is *k-compressible* in a certain basis, meaning that only the first k components, with $k \ll M$, condense all the significant information about the system behaviour. The manner in which this basis is determined gives the particular features of the ROM formulation. The concept of *k-compressibility* of the signals is therefore highly important. Next, we focus on the POD-ROM, which is classified as an *a posteriori* technique.

Remark. In what follows, all the HROMs which use a fixed frame of reference with respect to the welded piece, are based on the HF model given by Eq. (21). This choice is justified by considerations given in Section 4.2.

3.1. The Proper Orthogonal Decomposition approach

In an *a posteriori* approach, the response of the system is assumed to be known in advance, e.g., by running a training problem or performing experimental tests. Assuming that the response is k-compressible, we look for a procedure to build a basis $\boldsymbol{\Theta}$ for $\mathbb{R}^N$ with the peculiarity that only the first $k \ll N$ vectors of the basis provide significant information to reproduce the system response. From a physical point of view, we hope to be able to capture the dynamics of the problem with a reduced number of basis vectors. Solutions to problems similar to that of the training problem lie in $span\{\boldsymbol{\Theta}\}$. However, if we take into account that the first k vectors of the basis $\boldsymbol{\Theta}$ condense the significant information on the problem dynamics, we can form a reduced basis $\boldsymbol{\Xi}$ with only k of these vectors, and subsequently look for the solution in $span\{\boldsymbol{\Xi}\}$.

To build the basis, we proceed in a manner similar to that of Principal Component Analysis (PCA) [26]. The main objective is to reduce the dimensionality of the solution while retaining as much information as possible about the system response. To achieve this goal, first, a set of *snapshots* is built using time instances of the spatial distribution of the solution of the training problem [27]. Next, PCA is carried out by making use of the Proper Orthogonal Decomposition, better known in the context of linear algebra as Singular Value Decomposition (SVD) [28].

Remark. When non-homogeneous essential boundary conditions T_d are imposed, snapshots of the form $T^h - T_d$ are considered. In what follows, it is assumed for conciseness and without loss of generality that $T_d = 0$. The implementation of non-homogeneous essential boundary conditions is left for detailed analysis in a future work. It is taken into account that when $T_d = 0$, the trial and test function spaces are the same.

Let matrix $\boldsymbol{A}$ be a matrix formed by the set of collected snapshots. From the SVD, we have

$$\boldsymbol{A} = \boldsymbol{U}\boldsymbol{\Sigma}\boldsymbol{V}^T, \tag{23}$$

where the columns $\boldsymbol{u}$ of $\boldsymbol{U}$ are the left singular vectors of $\boldsymbol{A}$, the columns $\boldsymbol{v}$ of $\boldsymbol{V}$ are the right singular vectors of $\boldsymbol{A}$ and the diagonal entries σ of $\boldsymbol{\Sigma}$ are the singular values of $\boldsymbol{A}$. If the snapshots $\boldsymbol{A}$ correspond to a function $T_{sp}(\boldsymbol{x}, t)$, with $\boldsymbol{A}_{ij} = T_{sp}(\boldsymbol{x}_i, t_j)$, from Eq. (23) we have

$$T_{sp}(\boldsymbol{x}_i, t_j) = \left[\sum_{j=1}^{M} \boldsymbol{u}_j \otimes \boldsymbol{v}_j \, \sigma_j\right]_i. \tag{24}$$

If the response of the system is *k-compressible* with respect to the basis $\boldsymbol{u}_j$, we can write

$$T_{sp}(\boldsymbol{x}_i, t_j) \simeq \left[\sum_{j=1}^{k} \boldsymbol{u}_j \otimes \boldsymbol{v}_j \, \sigma_j\right]_i, \tag{25}$$

where $k \ll M$, and then, the separate representation given by Eq. (22) can be used to describe T^h in terms of $\boldsymbol{u}_j$, leading to

$$[\boldsymbol{T}_n]_i = T^h(\boldsymbol{x}_i, t_n) \simeq \left[\sum_{j=1}^{k} \boldsymbol{u}_j R_j(t_n)\right]_i. \tag{26}$$

In matrix notation, this equation is given in a more compact form by

$$T^h(\boldsymbol{x}, t_n) = \boldsymbol{N}^T \boldsymbol{T}_n = \boldsymbol{N}^T \boldsymbol{X} \boldsymbol{a}_n, \tag{27}$$

where $\boldsymbol{X}$ denotes the change of basis matrix whose columns are the first k vectors $\boldsymbol{u}_j$ and $\boldsymbol{a}_n$ denotes the vector of coefficients $R_j(t)$ evaluated at the time instant t_n.

From Eqs. (26) and (27), it can be concluded that the basis sought is given by the vectors $\boldsymbol{u}_j$ (commonly referred to as POD modes of the approximation). Moreover, the test functions v^h in this new basis are given by

$$v^h = \boldsymbol{N}^T \boldsymbol{X} \boldsymbol{\eta}, \tag{28}$$

with $\boldsymbol{\eta} \in \mathbb{R}^k$.

Making use of the test functions given by the last equation and using a Bubnov–Galerkin projection, we arrive at discrete variational formulation whose residual is given by

$$\boldsymbol{\Pi}_n^p = \boldsymbol{\Pi}^p(\boldsymbol{a}_n) = \boldsymbol{X}^T \boldsymbol{\Pi}(\boldsymbol{X}\boldsymbol{a}_n) = \boldsymbol{X}^T \frac{\boldsymbol{H}_n^c - \boldsymbol{H}_{n-1}^c}{\Delta t} + \boldsymbol{X}^T \boldsymbol{G}_n^k + \boldsymbol{X}^T \frac{\boldsymbol{H}_n^l - \boldsymbol{H}_{n-1}^l}{\Delta t} + \boldsymbol{X}^T \boldsymbol{F}_n - \boldsymbol{X}^T \boldsymbol{Q}_n = \boldsymbol{0}. \tag{29}$$

This result is equivalent to that obtained by projecting the residual given by Eq. (21) in the space spanned by $\boldsymbol{X}$; therefore, we refer to the modes $\boldsymbol{u}_j$ as projection modes of the approximation. Due to the high nonlinearity of the problem, a line-search method must be applied in conjunction with a Newton–Raphson scheme. This type of globally convergent method is quite standard and its formulation can be found in most textbooks in nonlinear optimisation [29,30].

The tangent matrix corresponding to the residual given by Eq. (29) is

$$\frac{\partial \boldsymbol{\Pi}_n^p}{\partial \boldsymbol{a}_n} = \boldsymbol{X}^T \frac{\partial \boldsymbol{\Pi}_n}{\partial \boldsymbol{a}_n} = \boldsymbol{X}^T \frac{\partial \boldsymbol{\Pi}_n}{\partial \boldsymbol{T}_n} \frac{\partial \boldsymbol{T}_n}{\partial \boldsymbol{a}_n} = \boldsymbol{X}^T \frac{\partial \boldsymbol{\Pi}_n}{\partial \boldsymbol{T}_n} \boldsymbol{X}. \tag{30}$$

As can be observed from the last equation, the system of equations to be solved in the ROM is much smaller in size than the system to be solved in the HF model. In the former case, the size of the problem is $k \times k$, and in the latter case, the size is $N \times N$. Although the computational cost of solving the system of linear equations is reduced, the cost of assembling the residual and the tangent matrix in each Newton iteration is still $O(N)$. To significantly reduce the computational cost, we must reduce the cost of assembling the residual and the tangent matrix at each Newton iteration. In the following sections, we introduce approximations that lead to the formulation of the so-called *hyper-reduced models*.

3.2. Optimality and consistency

Carlberg et al. [11] introduced the notions of optimality and consistency to ensure that *good* approximations are obtained when designing ROMs. According to Carlberg et al. [11], "an approximation is said to be *consistent* if, when implemented without data compression, it introduces no additional error in the solution of the same problem for which data was acquired... The approximation is said to be *optimal* if it leads to approximated quantities that minimise some error measure".

The ROM presented in this work satisfies consistency because, when the POD basis is not truncated, T^h is in $span\{\boldsymbol{X}\}$, and the solution of the training problem is recovered. With respect to the optimality of the approximation, it must be mentioned that a Bubnov–Galerkin projection is optimal if the Jacobian or the tangent matrix of the system is symmetric positive definite (SPD). If it is not the case, a Petrov–Galerkin projection should be used [11]. In our ROM, we use a Bubnov–Galerkin projection despite the fact that the system tangent matrix is not SPD because non-symmetry is not large for typical phase change problems.

4. Formulation of the Hyper Reduced Order Model

To reduce the cost of assembling the residual and the tangent matrix, we apply the gappy data reconstruction method introduced by Everson and Sirovich [19] in the image processing community and applied by many other researchers in the computational mechanics community [16,31,32]. Specifically, suppose only n_s components $\hat{\boldsymbol{u}}$ of a vector $\boldsymbol{u}$ are known. The objective is to build an approximation $\tilde{\boldsymbol{u}}$ to $\boldsymbol{u}$, starting from the known components $\hat{\boldsymbol{u}}$.

First, a set of snapshots corresponding to $\boldsymbol{u}$ is collected. After computing the SVD of this set of snapshots, we obtain a set of POD modes for $\boldsymbol{u}$. Assume that only the first n_g modes are significant; these modes are referred to in this work as gappy modes and are given as columns of a matrix $\boldsymbol{\Psi}$. Therefore, an approximation to $\boldsymbol{u}$ can be written as

$$\boldsymbol{u} \simeq \boldsymbol{\Psi}\boldsymbol{b}. \tag{31}$$

Let us assume that we know only n_s values of $\boldsymbol{u}$. This situation is represented by multiplying Eq. (31) by the sampling matrix $\boldsymbol{R}$ of size $n_s \times N$, yielding

$$\hat{\boldsymbol{u}} = \boldsymbol{R}\boldsymbol{u} \simeq \boldsymbol{R}\boldsymbol{\Psi}\boldsymbol{b} = \widehat{\boldsymbol{\Psi}}\boldsymbol{b}, \tag{32}$$

where the operator $\hat{\bullet}$ denotes the sampling of $\bullet$. Subsequently, this problem can be stated as that of finding $\boldsymbol{b} \in \mathbb{R}^{n_g}$ such that

$$\boldsymbol{b} = \arg\min_{\boldsymbol{c}\in\mathbb{R}^{n_g}} \|\widehat{\boldsymbol{\Psi}}\boldsymbol{c} - \widehat{\boldsymbol{u}}\|_2. \tag{33}$$

To get a unique solution, we require the columns of $\widehat{\boldsymbol{\Psi}}$ to be linearly independent. For this requirement to hold, the constraint $n_g \leqslant n_s$ must be met. Problem (33) subsequently can be solved either by computing the Moore–Penrose pseudo-inverse or by applying the QR decomposition. The latter technique is recommended for ill-conditioned matrices $\widehat{\boldsymbol{\Psi}}^T\widehat{\boldsymbol{\Psi}}$ [33]. In our problems, we have observed that although the condition of $\widehat{\boldsymbol{\Psi}}^T\widehat{\boldsymbol{\Psi}}$ could be somehow deteriorated in certain cases, the results obtained by applying either the QR decomposition or the pseudo-inverse did not differ significantly. In this work the pseudo-inverse is used, giving

$$\boldsymbol{b} = (\widehat{\boldsymbol{\Psi}}^T\widehat{\boldsymbol{\Psi}})^{-1}\widehat{\boldsymbol{\Psi}}^T\hat{\boldsymbol{u}}. \tag{34}$$

By replacing this result into Eq. (31), we arrive at

$$\boldsymbol{u} \simeq \tilde{\boldsymbol{u}} = \boldsymbol{\Psi}(\widehat{\boldsymbol{\Psi}}^T\widehat{\boldsymbol{\Psi}})^{-1}\widehat{\boldsymbol{\Psi}}^T\hat{\boldsymbol{u}}. \tag{35}$$

In other words, an approximation to the entire vector $\boldsymbol{u}$ is reconstructed, with only the knowledge of the n_s components $\hat{\boldsymbol{u}}$ of $\boldsymbol{u}$. By extending these ideas to our problem, we can compute the residual $\boldsymbol{\Pi}_n$ only knowing its values at n_s points, thus reducing the order of the assembly process from N to n_s, with $n_s \ll N$.

Several techniques aimed at finding the n_s points for which to evaluate $\boldsymbol{\Pi}_n$ have been proposed in the literature. A number of techniques operate at the discrete level, whereas others are expressed at the continuum level. Currently, two approaches that operate at the continuum level are widely used and can be mentioned: the *Best Point Interpolation Method* (*BPIM*) [34], which optimally selects the points, and the *Empirical Interpolation Method* (*EIM*) [35], which yields good but not optimal performance. Discrete versions of these algorithms have also been proposed [15,16]. This work uses an extension of the *Discrete Empirical Interpolation Method* (*DEIM*) [16]. This method is briefly described in Algorithm 1, in which the sampling points are returned in vector $\boldsymbol{p}$.

Algorithm 1. DEIM extension: return sampling points in vector $\boldsymbol{p}$

```
1: function DEIMEXT(Ψ)
2:     z := Ψ(:, 1)
3:     p(1) := maxAbs (z)                ▷ Find index of maximum absolute value of z
4:     for i = 1 to n_s − 1 do
5:         n := min (i, n_g)
6:         Λ := Ψ(p, 1 : n)
7:         U := Λ^T Λ
8:         v := mod (i, n_g) + 1
9:         z := Ψ(:, v)
10:        c := U^{-1} Λ^T z(p)
11:        r := z − Ψ(:, 1 : n)c
12:        p(i + 1) := maxAbs (r, p)     ▷ Find index of maximum absolute value
13:                                      ▷ of r which is not in the set of indices p
14:    end for
15:    return p
16: end function
```

Different approaches for the design of HROMs have been proposed in the literature [11,14,16,31,35,32]. The main differences among them lie in the choice of the set of snapshots used to compute the POD modes of the approximation. In addition, the proposal of Carlberg et al. [11,14] differs from the others in the fact that they use one set of POD modes for interpolating the residual and another set for interpolating the tangent matrix. Instead, in our proposal, we derive the method for interpolation of the tangent matrix from the procedure used to interpolate the residual. For this reason, we first focus our study on the treatment of the residual.

In the following sections, two different approximations for collecting the snapshots are analysed. The expected performance of each approximation is evaluated in terms of the *Relative Information Content* (*RIC*), indicator, which is defined as

$$\mathrm{RIC} = \frac{\sum_{i=1}^{N_s} \lambda_i}{\sum_{i=1}^{N_r} \lambda_i}, \tag{36}$$

where λ_i are the singular values of the SVD, N_s is the number of singular values kept in the truncation and N_r is the total number of singular values of the SVD.

4.1. Snapshot collection by one nucleating nonlinear term

A strategy used to formulate the HROM divides the residual into two contributions: one term that nucleates the linear terms and another that nucleates the nonlinear terms [31]. Next, the gappy method is applied to the nonlinear term. In this sense, it can be said that the residual is divided into one term, which is hyper-reduced, and another term, which is assembled just once without needing to be hyper-reduced. Certain other authors, such as Carlberg et al. [11,14], hyper-reduce the residual as a single entity.

In our case, the terms that comprise the residual $\boldsymbol{\Pi}_n$ in Eq. (21) are all nonlinear except for the heat source term. However, because the heat source is in motion and follows a given trajectory, an assembly process is required for this term at each time instant, operation which is $O(N)$. Therefore, this term also must be hyper-reduced by gappy data reconstruction, making it necessary to hyper-reduce the residual as a unit, similar to what was performed by Carlberg et al.

We take the residuals of the HF model in each Newton iteration as snapshots, diverging from Carlberg et al. at this point because they take the residuals of the reduced problem as snapshots instead (formulation presented in Section 3.2). The POD modes for interpolation are computed by applying the SVD to the set of collected snapshots. If we denote $\boldsymbol{\Phi}$ the first n_g POD modes of the residual, we have

$$\boldsymbol{\Pi}_n \simeq \widetilde{\boldsymbol{\Pi}}_n = \boldsymbol{\Phi}(\widehat{\boldsymbol{\Phi}}^T\widehat{\boldsymbol{\Phi}})^{-1}\widehat{\boldsymbol{\Phi}}^T\widehat{\boldsymbol{\Pi}}_n. \tag{37}$$

Next, to obtain the hyper-reduced residual $\boldsymbol{\Pi}_n^p$, we project this equation with the POD basis $\boldsymbol{X}$ as in Eq. (29); that is

$$\boldsymbol{\Pi}_n^p = \boldsymbol{X}^T\widetilde{\boldsymbol{\Pi}}_n = \boldsymbol{X}^T\boldsymbol{\Phi}(\widehat{\boldsymbol{\Phi}}^T\widehat{\boldsymbol{\Phi}})^{-1}\widehat{\boldsymbol{\Phi}}^T\widehat{\boldsymbol{\Pi}}_n = \boldsymbol{A}_r\widehat{\boldsymbol{\Pi}}_n. \tag{38}$$

Take into account that matrix $\boldsymbol{A}_r = \boldsymbol{X}^T\boldsymbol{\Phi}(\widehat{\boldsymbol{\Phi}}^T\widehat{\boldsymbol{\Phi}})^{-1}\widehat{\boldsymbol{\Phi}}^T$ is computed just once in the *off-line* stage.

The hyper-reduced tangent matrix is finally obtained by differentiation of the last equation to produce

$$\frac{\partial\boldsymbol{\Pi}_n^p}{\partial\boldsymbol{a}_n} = \boldsymbol{A}_r\frac{\partial\widehat{\boldsymbol{\Pi}}_n}{\partial\boldsymbol{a}_n} = \boldsymbol{A}_r\frac{\partial\boldsymbol{R}\boldsymbol{\Pi}_n}{\partial\boldsymbol{a}_n} = \boldsymbol{A}_r\boldsymbol{R}\frac{\partial\boldsymbol{\Pi}_n}{\partial\boldsymbol{T}_n}\boldsymbol{X}. \tag{39}$$

Remark

- If all modes are retained in the gappy basis $\boldsymbol{\Phi}$ and in the basis $\boldsymbol{X}$, i.e., $\boldsymbol{\Phi} = \widehat{\boldsymbol{\Phi}}$ and $\boldsymbol{\Pi}_n = \widehat{\boldsymbol{\Pi}}_n$, then in Eq. (37) produces

$$\widetilde{\boldsymbol{\Pi}}_n = \boldsymbol{\Phi}(\boldsymbol{\Phi}^T\boldsymbol{\Phi})^{-1}\boldsymbol{\Phi}^T\boldsymbol{\Pi}_n = \boldsymbol{\Phi}\boldsymbol{I}^{-1}\boldsymbol{\Phi}^T\boldsymbol{\Pi}_n = \boldsymbol{\Phi}\boldsymbol{\Phi}^T\boldsymbol{\Pi}_n = \boldsymbol{I}\boldsymbol{\Pi}_n = \boldsymbol{\Pi}_n, \tag{40}$$

where $\boldsymbol{I}$ is the identity matrix. Therefore, when no truncation is carried out, the residual $\boldsymbol{\Pi}_n$ is fully recovered. Using this result in Eq. (38), the projected residual given by Eq. (29) is obtained, and the solution of the HROM and the solution of the ROM coincide. Moreover, it was shown in Section 3.2 that the solution of the ROM converges to the solution of the training problem when no truncation is used, making it possible to conclude that the solution of the HROM and the solution of the training problem are the same, and therefore the method is consistent.
- To ensure that the projected tangent matrix given by Eq. (39) is full-rank, we require the number of gappy modes n_g to obey the constraint $n_g \geqslant k$. The justification for this constraint is given in Section 4.3.
- Eq. (38) can be re-written as

$$\boldsymbol{\Pi}_n^p = \boldsymbol{X}^T\boldsymbol{\Phi}\boldsymbol{d}_n, \tag{41}$$

where $\boldsymbol{d}_n$ is the vector that condenses the rest of the terms involved in the HROM. Next, it is evident that matrix $\boldsymbol{X}^T\boldsymbol{\Phi}$ should have rank k for the formulation of the HROM to be well-posed. This condition is satisfied by the current hyper-reduced formulation, and details are given in Section 4.3.

- The columns of $\boldsymbol{\Phi}$ are left singular vectors of the SVD of the matrix built by the snapshots taken at all Newton iterations of the residual. Therefore, they should normally be linearly independent, which is the condition required for $\boldsymbol{\Phi}$ to be a basis. However, in certain cases, these vectors can be close to parallel. An example is a case in which snapshots are collected from a training problem with a notably small time step; in this situation, all residuals will be close to zero and the computed left singular vectors will be almost linearly dependent. This type of situations leads to ill-conditioning and problems of convergence.

4.2. Snapshot collection by individual nonlinear terms

An alternative approach for the snapshot collection is proposed in this section to avoid the inconveniences of the previous procedure. We consider the residual $\boldsymbol{\Pi}_n$ as the summation of various physically based nonlinear generalised contributing forces plus one term that nucleates the linear contributions. Next, each nonlinear term will be individually stored and hyper-reduced. The heat source term will be hyper-reduced as well to reduce its assembly cost from $O(N)$ to $O(n_s)$.

To obtain an optimal method, we need to individualise terms that are highly *compressible*. Two forms of the discrete thermal nonlinear problem were proposed in Section 2.1: Eqs. (13) and (21). The difference between them lies in the way the capacitance and latent heat forces are handled.

The SVD spectrum of $\boldsymbol{G}_n^c$ and $\boldsymbol{G}_n^l$ in Eq. (13) is less compact than that of the terms $\boldsymbol{H}_n^c$ and $\boldsymbol{H}_n^l$ because the latter terms can be viewed as integrated forms of the former. Indeed, this was verified by numerical experiments. Moreover, it was verified that the condition of the HROM tangent matrix in the former case is worse than in the latter case. For these reasons, the formulation given by Eq. (21) was adopted, instead of that given by Eq. (13), as HF model for the HROM.

Each term of Eq. (21) has an associated POD basis for its gappy data reconstruction. In what follows, suffixes $i \in \{c,k,l,f,q\}$ are used to identify the different POD bases $\boldsymbol{\Phi}_i$ and sampling matrices $\boldsymbol{R}_i$, corresponding to each term. We emphasise that the sampling matrices are different for each term, but the number of sampling points n_s and the number of gappy modes n_g are always the same for all. Then, the approximation to each term from the gappy data reconstruction is given by

$$\boldsymbol{H}_n^c \simeq \boldsymbol{\Phi}_c \left(\widehat{\boldsymbol{\Phi}}_c^T \widehat{\boldsymbol{\Phi}}_c\right)^{-1} \widehat{\boldsymbol{\Phi}}_c^T \widehat{\boldsymbol{H}}_n^c, \tag{42}$$

$$\boldsymbol{G}_n^k \simeq \boldsymbol{\Phi}_k \left(\widehat{\boldsymbol{\Phi}}_k^T \widehat{\boldsymbol{\Phi}}_k\right)^{-1} \widehat{\boldsymbol{\Phi}}_k^T \widehat{\boldsymbol{G}}_n^k, \tag{43}$$

$$\boldsymbol{H}_n^l \simeq \boldsymbol{\Phi}_l \left(\widehat{\boldsymbol{\Phi}}_l^T \widehat{\boldsymbol{\Phi}}_l\right)^{-1} \widehat{\boldsymbol{\Phi}}_l^T \widehat{\boldsymbol{H}}_n^l, \tag{44}$$

$$\boldsymbol{F}_n \simeq \boldsymbol{\Phi}_f \left(\widehat{\boldsymbol{\Phi}}_f^T \widehat{\boldsymbol{\Phi}}_f\right)^{-1} \widehat{\boldsymbol{\Phi}}_f^T \widehat{\boldsymbol{F}}_n, \tag{45}$$

$$\boldsymbol{Q}_n \simeq \boldsymbol{\Phi}_q \left(\widehat{\boldsymbol{\Phi}}_q^T \widehat{\boldsymbol{\Phi}}_q\right)^{-1} \widehat{\boldsymbol{\Phi}}_q^T \widehat{\boldsymbol{Q}}_n, \tag{46}$$

where $\widehat{\cdot}$ denotes the vector of n_s components sampled from the associated full term.

To obtain the hyper-reduced residual $\boldsymbol{\Pi}_n^p$ we project the approximation of $\boldsymbol{\Pi}_n$ with the POD basis $\boldsymbol{X}$, as in Eq. (38) which results in

$$\boldsymbol{\Pi}_n^p = \boldsymbol{A}_c \frac{\widehat{\boldsymbol{H}}_n^c - \widehat{\boldsymbol{H}}_{n-1}^c}{\Delta t} + \boldsymbol{A}_k \widehat{\boldsymbol{G}}_n^k + \boldsymbol{A}_l \frac{\widehat{\boldsymbol{H}}_n^l - \widehat{\boldsymbol{H}}_{n-1}^l}{\Delta t} + \boldsymbol{A}_f \widehat{\boldsymbol{F}}_n - \boldsymbol{A}_q \widehat{\boldsymbol{Q}}_n, \tag{47}$$

where $\boldsymbol{A}_i = \boldsymbol{X}^T \boldsymbol{\Phi}_i (\widehat{\boldsymbol{\Phi}}_i^T \widehat{\boldsymbol{\Phi}}_i)^{-1} \widehat{\boldsymbol{\Phi}}_i^T$, with $i \in \{c,k,l,f,q\}$. Again, take into account that matrices $\boldsymbol{A}_i$ are computed in the *off-line* stage.

Finally, the hyper-reduced tangent matrix is obtained by differentiating the residual with respect to the global unknown parameters

$$\frac{\partial \boldsymbol{\Pi}_n^p}{\partial \boldsymbol{a}_n} = \boldsymbol{A}_c \boldsymbol{R}_c \frac{\partial \boldsymbol{H}_n^c}{\partial \boldsymbol{T}_n} \boldsymbol{X} + \boldsymbol{A}_k \boldsymbol{R}_k \frac{\partial \boldsymbol{G}_n^k}{\partial \boldsymbol{T}_n} \boldsymbol{X} + \boldsymbol{A}_l \boldsymbol{R}_l \frac{\partial \boldsymbol{H}_n^l}{\partial \boldsymbol{T}_n} \boldsymbol{X}. \tag{48}$$

The consistency of the current HROM can be shown by following the same procedure that was applied in the previous method (Section 4.1).

4.3. Relationship between the projection and the hyper-reduction spaces

In the previously developed HROMs, we addressed hyper-reduced quantities of the form $\boldsymbol{X}^T \boldsymbol{\Phi}_i \boldsymbol{d}_n$, where $\boldsymbol{X}$ is the basis spanning the solution space, $\boldsymbol{\Phi}_i$ is the POD basis used in the gappy data reconstruction and $\boldsymbol{d}_n$ is a vector condensing the rest of the terms involved in the HROM. To obtain a well-posed formulation of the HROM, we need matrix $\boldsymbol{X}^T \boldsymbol{\Phi}_i$ to have maximum rank k. Note that terms $\boldsymbol{\Phi}_i$ and $\boldsymbol{X}$ are energetically conjugated. Therefore, their mutual product is equal to an energy increment, and it is intuitively expected that $\boldsymbol{X}^T \boldsymbol{\Phi}_i$ has maximum rank k. Next, we show that this expectation is effectively verified in our case.

For the solidification problem under consideration, we take the temperature values $\boldsymbol{T}_j$ of the system at a sequence of S time instants $t_j,\ j = 1,\dots S$ as snapshots for building the basis $\boldsymbol{X}$. To design the HROM, we computed the residual as the summation of various physical contributions and took snapshots for each of these quantities to compute the corresponding POD basis for the gappy data reconstruction procedure.

For instance, let us consider the thermal conductivity term: the nonlinear contribution to the residual reads

$$\boldsymbol{G}_j^k = \int_\Omega \nabla \boldsymbol{N} \cdot (k\, \nabla \boldsymbol{N}\, \boldsymbol{T}_j)\, d\Omega. \tag{49}$$

For the problem at hand, it is well known that

$$\int_\Omega \nabla \boldsymbol{T}_j \cdot (k \nabla \boldsymbol{T}_j)\, d\Omega = \boldsymbol{T}_j^T \boldsymbol{K} \boldsymbol{T}_j \ > \ 0 \tag{50}$$

with given Dirichlet boundary conditions. If we assume that the temperature field signal is *k-compressible*, we know that for a certain basis $\boldsymbol{X}$ there exists $\xi_j \in \mathbb{R}^k$ such that

$$\boldsymbol{T}_j = \boldsymbol{X}\xi_j, \tag{51}$$

where the equality is used for conciseness (it is in fact $\boldsymbol{T}_j \simeq \boldsymbol{X}\xi_j$).

Now, let $\boldsymbol{B} = \left[\boldsymbol{G}_1^k, \boldsymbol{G}_2^k, \dots, \boldsymbol{G}_S^k\right]$ denote the matrix formed by S snapshots $\boldsymbol{G}_j^k = \boldsymbol{K}\boldsymbol{T}_j$. If we assume that $\boldsymbol{B}$ is n_g-*compressible* and $n_g \geqslant k$, we have

$$\boldsymbol{B}\boldsymbol{B}^T = \boldsymbol{\Phi}_k \boldsymbol{\Lambda}^2 \boldsymbol{\Phi}_k^T, \tag{52}$$

where $\boldsymbol{\Lambda}$ is the matrix of the first n_g singular values of $\boldsymbol{B}$, and $\boldsymbol{\Phi}_k$ are the first n_g left singular vectors of $\boldsymbol{B}$.

Let us now consider matrix $\boldsymbol{C}$ defined as the projection of $\boldsymbol{B}^T\boldsymbol{B}$ on the solution space. From the considerations above, we obtain

$$\boldsymbol{C} = \boldsymbol{X}^T \boldsymbol{\Phi}_k \boldsymbol{\Lambda}^2 \boldsymbol{\Phi}_k^T \boldsymbol{X} = \boldsymbol{X}^T \boldsymbol{B}\boldsymbol{B}^T \boldsymbol{X} = \boldsymbol{X}^T \boldsymbol{K}\boldsymbol{J}\boldsymbol{J}^T \boldsymbol{K}^T \boldsymbol{X}, \tag{53}$$

where $\boldsymbol{J} = [\boldsymbol{T}_1, \boldsymbol{T}_2, \dots, \boldsymbol{T}_S]$. The term $\boldsymbol{J}\boldsymbol{J}^T$ can be expressed as

$$\boldsymbol{J}\boldsymbol{J}^T = \boldsymbol{X}\boldsymbol{\Sigma}^2 \boldsymbol{X}^T, \tag{54}$$

because the temperature field is assumed to be *k-compressible*, where $\boldsymbol{\Sigma}$ is the matrix of the first k singular values of $\boldsymbol{J}$. Therefore, $\boldsymbol{C}$ reads

$$\boldsymbol{C} = \boldsymbol{X}^T \boldsymbol{K}\boldsymbol{X}\boldsymbol{\Sigma}^2 \boldsymbol{X}^T \boldsymbol{K}^T \boldsymbol{X} = \overline{\boldsymbol{K}}^T \boldsymbol{\Sigma}^2 \overline{\boldsymbol{K}}, \tag{55}$$

where $\overline{\boldsymbol{K}} = \boldsymbol{X}^T \boldsymbol{K}^T \boldsymbol{X}$. From Eq. (50), $\overline{\boldsymbol{K}}$ is symmetric positive definite. Moreover, if the left singular vectors associated with zero singular values are not part of $\boldsymbol{X}$, $\boldsymbol{\Sigma}^2$ is a diagonal matrix with positive entries. Therefore, $\boldsymbol{C}$ is symmetric positive definite and invertible. It follows therefore that the matrix $\boldsymbol{X}^T\boldsymbol{\Phi}_k$ has rank k.

A similar analysis can be carried for the other terms of the HROM presented in Section 4.2 with the conclusion that it is well-posed. A similar conclusion can be obtained for the HROM given in Section 4.1.

We mention for completeness that an HROM formulation in which the projection space and the hyper-reduction space are mutually orthogonal leads to an ill-posed problem. A solution to this type of singularity was proposed by Hernández et al. [13].

It was previously mentioned that to ensure the projected tangent matrix is full-rank, the number of gappy modes must obey the constraint $n_g \geqslant k$. The reason for this constraint is obvious with the development presented in this section. If the number of gappy modes is smaller than the number of POD projection modes, i.e., $n_g < k$, the matrix $\boldsymbol{B}\boldsymbol{B}^T$ given by Eq. (52) would have rank n_g, and the invertibility of $\boldsymbol{C}$ would not be guaranteed, and it cannot be assured that the projected tangent matrix would have rank k.

5. Alternative formulation: the moving frame approach

A formulation of HROMs for nonlinear transient heat conduction problems expressed in terms of a moving frame of reference is introduced next, specifically, a frame of reference attached to a heat source. In the case of a highly concentrated moving heat source, such a formulation permits us to obtain a problem whose solution is characterised by a high *compressibility*. In other words, a small number of projection modes and gappy points are required when using a moving frame of reference that follows the high gradients present in the solution.

5.1. Variational formulation and discretisation

The following considers the energy balance equations in a moving frame of reference attached to the heat source. Let $\boldsymbol{e}_i$, with $i \in \{1,2,3\}$, be unit vectors associated with a body fixed frame centered at O. Let $\boldsymbol{r}(t)$ be the parametrisation of the

curve describing the trajectory of the heat source with respect to $\boldsymbol{e}_i$. We describe this trajectory by the position of M_c points $\boldsymbol{c}_i$, interpolated by shape functions $R_i(t)$

$$\boldsymbol{r}(t) = \sum_{i=1}^{M_c} R_i(t)\boldsymbol{c}_i, \tag{56}$$

where the time $t \in [0, t_f]$ is subdivided into $M_c - 1$ sub-intervals $I_k = (t_k, t_{k+1})$ with $k \in \{1, \ldots, M_c - 1\}$, such that $\boldsymbol{r}(t_k) = \boldsymbol{c}_k$.

In the case of a moving frame, Fig. 2, the position of the heat source at each time instant is taken as the origin of this moving welding frame or the position of the observer O'. We denote by $\boldsymbol{u}_i$, with $i \in \{1, 2, 3\}$, the orthonormal unit vectors associated to the moving frame. We use a cubic spline to interpolate the trajectory of the heat source. Let $\boldsymbol{p}_s$ and $\boldsymbol{p}_e$ be the given starting tangent at $t = 0$ and the given ending tangent at $t = t_f$, respectively. Next, $\boldsymbol{r}(t)$ in an arbitrary interval I_k is given by

$$\boldsymbol{r}(t) = R_{00}(t)\boldsymbol{c}_k + R_{10}(t)\boldsymbol{p}_k + R_{01}(t)\boldsymbol{c}_{k+1} + R_{11}(t)\boldsymbol{p}_{k+1}, \tag{57}$$

where

$$R_{00}(t) = (1 + 2\zeta)(1 - \zeta)^2, \tag{58}$$
$$R_{10}(t) = (t - t_k)(1 - \zeta)^2, \tag{59}$$
$$R_{01}(t) = (3 - 2\zeta)\zeta^2, \tag{60}$$
$$R_{11}(t) = (t - t_k)(1 - \zeta)\zeta, \tag{61}$$
$$\zeta = \frac{t - t_k}{t_{k+1} - t_k}. \tag{62}$$

The tangents $\boldsymbol{p}_k$ are computed according to the Catmull–Rom formula

$$\boldsymbol{p}_k = \frac{\boldsymbol{p}_{k+1} - \boldsymbol{p}_{k-1}}{t_{k+1} - t_{k-1}}. \tag{63}$$

The unit vectors $\boldsymbol{u}_i$ of the welding frame are given by (i) $\boldsymbol{u}_1(t) = \boldsymbol{r}'(t)/\|\boldsymbol{r}'(t)\|$ the tangent to the trajectory; (ii) $\boldsymbol{u}_2(t)$ the outward normal to the welding surface; and (iii) $\boldsymbol{u}_3(t) = \boldsymbol{u}_1(t) \times \boldsymbol{u}_2(t)$. The set of coordinates in this frame is denoted by $\boldsymbol{\xi} = [\xi_1, \xi_2, \xi_3]$.

The position vector $\boldsymbol{p}$ of an arbitrary point $\boldsymbol{Y}$ with respect to the fixed frame O can be computed as

$$\boldsymbol{p}(t) = \boldsymbol{o}(t) + \boldsymbol{\Lambda}(t)\boldsymbol{q}(t), \tag{64}$$

where $\boldsymbol{q}(t)$ is the position of $\boldsymbol{Y}$ with respect to the moving frame O', vector $\boldsymbol{o}(t)$ is the position of the moving frame with respect to the fixed frame and $\boldsymbol{\Lambda}$ is the rotation matrix formed by the unit vectors $\boldsymbol{u}_i$ as columns.

The material derivative in the moving frame of the scalar field T is given by

$$\frac{DT}{Dt} = \frac{\partial T}{\partial t} + \frac{\partial \boldsymbol{\xi}}{\partial t} \cdot \nabla_\xi T, \tag{65}$$

where ∇_ξ is the gradient operator given by $\nabla_\xi = \frac{\partial}{\partial \boldsymbol{\xi}}$, and

$$\frac{\partial \boldsymbol{\xi}}{\partial t} = \frac{\partial \boldsymbol{\Lambda}^T}{\partial t}\boldsymbol{\Lambda}\boldsymbol{q} - \boldsymbol{\Lambda}^T\frac{\partial \boldsymbol{o}}{\partial t}. \tag{66}$$

The Jacobian of the transformation relating both frames is given by

$$\frac{\partial \boldsymbol{\xi}}{\partial \boldsymbol{x}} = \boldsymbol{\Lambda} \tag{67}$$

and therefore, the conductivity term reads

$$\nabla \cdot \boldsymbol{k}\nabla T = \nabla_\xi \cdot (\boldsymbol{\Lambda}\boldsymbol{k}\boldsymbol{\Lambda}^T)\nabla_\xi T. \tag{68}$$

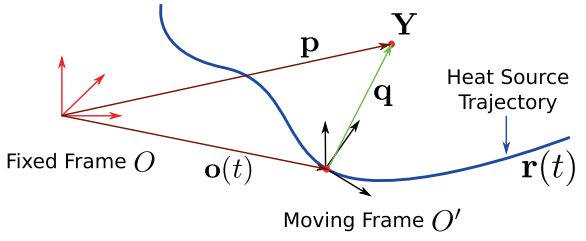

Fig. 2. Fixed and moving frames.

The material derivative of the liquid fraction is analysed next. Note that this term must be understood in a distributional sense. The material derivative of the liquid fraction in a variational framework can be expressed as

$$\int_\Omega w \frac{Df_l}{Dt}\, d\Omega = \int_\Omega w \left[\frac{\partial f_l}{\partial t} + \frac{\partial \boldsymbol{\xi}}{\partial t}\cdot \nabla_\xi f_l\right] d\Omega. \tag{69}$$

By applying Green's theorem to the second term, we obtain

$$\int_\Omega w \frac{\partial \boldsymbol{\xi}}{\partial t}\cdot \nabla_\xi f_l\, d\Omega = -\int_\Omega f_l \frac{\partial \boldsymbol{\xi}}{\partial t}\cdot \nabla_\xi w\, d\Omega - \int_\Omega f_l w \nabla_\xi \cdot \frac{\partial \boldsymbol{\xi}}{\partial t}\, d\Omega + \int_{\Gamma\setminus\Gamma_d} f_l w \frac{\partial \boldsymbol{\xi}}{\partial t}\cdot \boldsymbol{n}\, d\Gamma. \tag{70}$$

Taking into account that $\nabla_\xi \cdot \frac{\partial \boldsymbol{\xi}}{\partial t} = 0$ and that $\frac{\partial \boldsymbol{\xi}}{\partial t}\cdot \boldsymbol{n} = 0$, because the torch motion lies on the body surface, we obtain

$$\int_\Omega w \frac{\partial \boldsymbol{\xi}}{\partial t}\cdot \nabla_\xi f_l\, d\Omega = -\int_\Omega f_l \frac{\partial \boldsymbol{\xi}}{\partial t}\cdot \nabla_\xi w\, d\Omega. \tag{71}$$

Finally, the variational formulation for the welding problem expressed in a frame moving with the heat source reads:
Find $T \in \mathcal{S}$ such that $\forall w \in \mathcal{V}$

$$\begin{aligned}&\int_\Omega w\left[\rho c \frac{\partial T}{\partial t} + \rho c \frac{\partial \boldsymbol{\xi}}{\partial t}\cdot \nabla_\xi T + \rho \mathcal{L} \frac{\partial f_l}{\partial t} - Q(\xi)\right] d\Omega + \int_\Omega \nabla_\xi w \cdot \left[(\boldsymbol{\Lambda k \Lambda}^T)\nabla_\xi T - \rho \mathcal{L} f_l \frac{\partial \boldsymbol{\xi}}{\partial t}\right] d\Omega \\ &\quad + \int_{\Gamma_c} w h_f (T - T_f)\, d\Gamma + \int_{\Gamma_q} w q_w\, d\Gamma = 0, \quad \text{for } t > 0; \\ &\int_\Omega wT\, d\Omega = \int_\Omega wT_0\, d\Omega, \quad \text{for} \quad t = 0.\end{aligned} \tag{72}$$

Note that in this case the heat source $Q(\xi)$ does not depend on time. Note also that two new terms appear compared with Eq. (11): one originating from the material time derivative of the temperature field and another from the material time derivative of the liquid fraction. Additionally, the conductivity properties are affected by the rotation of the computation frame.

The finite element discretisation is quite similar to the one introduced in Section 2.1. The equation to be solved is briefly expressed as

$$\boldsymbol{\Pi}_n = \frac{\boldsymbol{H}^c_n - \boldsymbol{H}^c_{n-1}}{\Delta t} + \boldsymbol{G}^k_n + \boldsymbol{G}^{vc}_n + \frac{\boldsymbol{H}^l_n - \boldsymbol{H}^l_{n-1}}{\Delta t} - \boldsymbol{G}^{vl}_n + \boldsymbol{F}_n - \boldsymbol{Q} = \boldsymbol{0}, \tag{73}$$

where the new term $\boldsymbol{G}^{vc}_n$ is taken from the discretisation of the term $\rho c \frac{\partial \boldsymbol{\xi}}{\partial t}\cdot \nabla_\xi T$, and $\boldsymbol{G}^{vl}_n$ expresses the discretisation of the term $\nabla_\xi w \cdot \rho \mathcal{L} f_l \frac{\partial \boldsymbol{\xi}}{\partial t}$.

5.2. HROM formulation

The HROM formulation in the moving frame is constructed using the same developments as for the fixed frame formulation. The procedure for dividing the residual $\boldsymbol{\Pi}_n$ into a set of physically based nonlinear generalised forces that contribute to the residual and one term that nucleates the linear contributions, is followed. Next, the only difference is that the hyper-reduced versions of the new terms $\boldsymbol{G}^{vc}_n$ and $\boldsymbol{G}^{vl}_n$ must be incorporated, resulting in

$$\boldsymbol{\Pi}^p_n = \boldsymbol{A}_c \frac{\widehat{\boldsymbol{H}}^c_n - \widehat{\boldsymbol{H}}^c_{n-1}}{\Delta t} + \boldsymbol{A}_{vc}\widehat{\boldsymbol{G}}^{vc}_n + \boldsymbol{A}_k \widehat{\boldsymbol{G}}^k_n + \boldsymbol{A}_l \frac{\widehat{\boldsymbol{H}}^l_n - \widehat{\boldsymbol{H}}^l_{n-1}}{\Delta t} - \boldsymbol{A}_{vl}\widehat{\boldsymbol{G}}^{vl}_n + \boldsymbol{A}_f \widehat{\boldsymbol{F}}_n - \boldsymbol{X}^T \boldsymbol{Q}. \tag{74}$$

Note that because the heat source term does not depend on time, it is not hyper-reduced and its projection is computed only once. In addition, note that the same notation of Section 5.2 has been used to identify the POD modes and the gappy modes. Clearly, these modes have been computed from snapshots obtained from a HF model calculated using a moving frame of reference formulation and therefore they are different from the modes used in Section 5.2.

6. Application examples

We present two examples for assessing the performance of the introduced HROMs. The first example consists of the solidification of a cube. In the second example, we study a welding-like problem of a tube without material deposition.

The HF model given by Eq. (21) was used in the formulation of the HROMs presented in Sections 4.1 and 4.2. Since both HROMs are based on the same HF formulation, results can be consistently compared. The HF model given by Eq. (73) was used in the moving frame formulation.

To assess the performance and robustness of the introduced HROMs, the following parameters are evaluated:

- The condition number of the matrices $\boldsymbol{M} = \widehat{\boldsymbol{\Phi}}^T_i \widehat{\boldsymbol{\Phi}}_i$ that are part of the gappy data reconstruction method. The condition number cond($\boldsymbol{M}$), is computed as

$$\mathrm{cond}(\boldsymbol{M}) = \frac{\lambda_e}{\lambda_0}, \tag{75}$$

where λ_0 and λ_e are the maximum and minimum singular values of $\boldsymbol{M}$, respectively.

- The evolution of the condition number of the HROM tangent matrix. This information is plotted in terms of the global iteration number (the iterations are numbered globally, i.e., the iterations of all time steps are consecutively numbered).
- The relative error ϵ introduced by the HROM. This error is computed as

$$\epsilon = \frac{\|T_R - T_H\|_F}{\|T_H\|_F}, \tag{76}$$

where T_R is the matrix of the solution in time obtained with the HROM, T_H is the HF solution for the same problem, and $\| \bullet \|_F$ is the Frobenius norm of matrix $\bullet$. To measure this error, the temperature field is computed for every 20 time steps of the simulation.

- The speedup S_H of the HROM with respect to the HF model, defined as

$$S_H = \frac{t_H}{t_R}, \tag{77}$$

where t_H and t_R are the total times needed to compute the solution by the HF model and by the HROM (online stage only), respectively. The computations were carried out by saving the results for every 20 time steps.

A normalised residual norm was used to verify convergence of the Newton–Raphson scheme, given in the HF case by

$$\frac{\|\boldsymbol{\Pi}_n\|}{\left\|\boldsymbol{G}_n^I\right\| + \left\|\boldsymbol{G}_n^k\right\| + \left\|\boldsymbol{G}_n^c\right\| + \|\boldsymbol{F}_n\| + \|\boldsymbol{Q}_n\|}, \tag{78}$$

where $\| \bullet \|$ denotes the L_2 norm of $\bullet$. The normalised residual norm for the HROM is defined similarly with the corresponding hyper-reduced quantities. Convergence of the Newton–Raphson scheme is verified when the normalised residual norm is below 1×10^{-6}.

The tests were performed in a computer with the following characteristics:

- Processors: 2 x [Intel(R) Xeon(R) CPU X5680 @ 3.33 GHz].
- Number of physical cores: 6 cores on each processor; hyper-threading deactivated.
- Cache L1, L2, L3: 32 KB, 256 KB, 12 MB.
- NUMA nodes #0, #1: 2 x 48 GB.
- Operating system: `Linux 3.5.1–1.fc17.x86_64 #1 SMP x86_64 x86_64 x86_64 GNU/Linux`.

6.1. Solidification of a cube

Solidification of a cube of side $L = 0.41$ m is analysed first. The body is located at the positive octant, with a corner at the origin of coordinates $(0,0,0)$. It is initially at constant temperature $T_0 = 2500$ K and is cooled from sides $s_1 = (0, y, z)$ and $s_2 = (x, 0, z)$. Cooling is described by means of a Robin boundary condition, with fluid temperature $T_f = 299$ K. The other sides of the cube are perfectly insulated. The heat capacity c, the thermal conductivity k and the heat convection coefficient h_f depend on the temperature and are given by the expressions

$$\begin{aligned} c\left[\frac{\mathrm{J}}{\mathrm{kg\,K}}\right] &= 0.19566T[\mathrm{K}] + 474.04, \\ k\left[\frac{\mathrm{W}}{\mathrm{m\,K}}\right] &= 0.011808T[\mathrm{K}] + 3.7066, \\ h_f\left[\frac{\mathrm{W}}{\mathrm{m^2\,K}}\right] &= 2.6T[\mathrm{K}] - 55. \end{aligned} \tag{79}$$

The material density is $\rho = 4430\frac{\mathrm{kg}}{\mathrm{m}}$, the solidus temperature is 1877 K, the liquidus temperature is 1933 K and the latent heat is $\mathcal{L} = 292600\frac{\mathrm{J}}{\mathrm{kg}}$. The geometry is discretised using 162000 equally spaced tetrahedra and 29791 degrees of freedom. A constant time step of 1 s is used for a simulation in the time interval $[0, 800]$ s. The computation of the HF solution required 4318.6 s of CPU time.

6.1.1. Results obtained by hyper-reducing the residual

The HROM presented in Section 4.1 is applied in this section to solve the solidifying cube problem. Fig. 3 shows the SVD spectrum of the temperature and of the residual histories. From this figure, a good approximation is expected using a small number of projection modes and sampling points. However, as shown in the following, this is not the case, and the error could not be decreased below 1×10^{-4}.

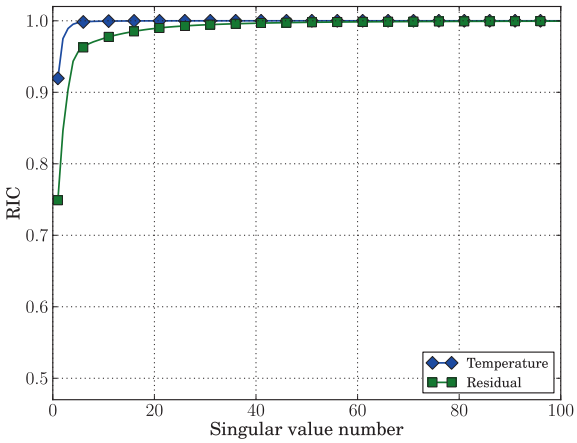

Fig. 3. Solidifying cube problem: hyper-reduction of the residual. SVD spectrum for each of the involved terms.

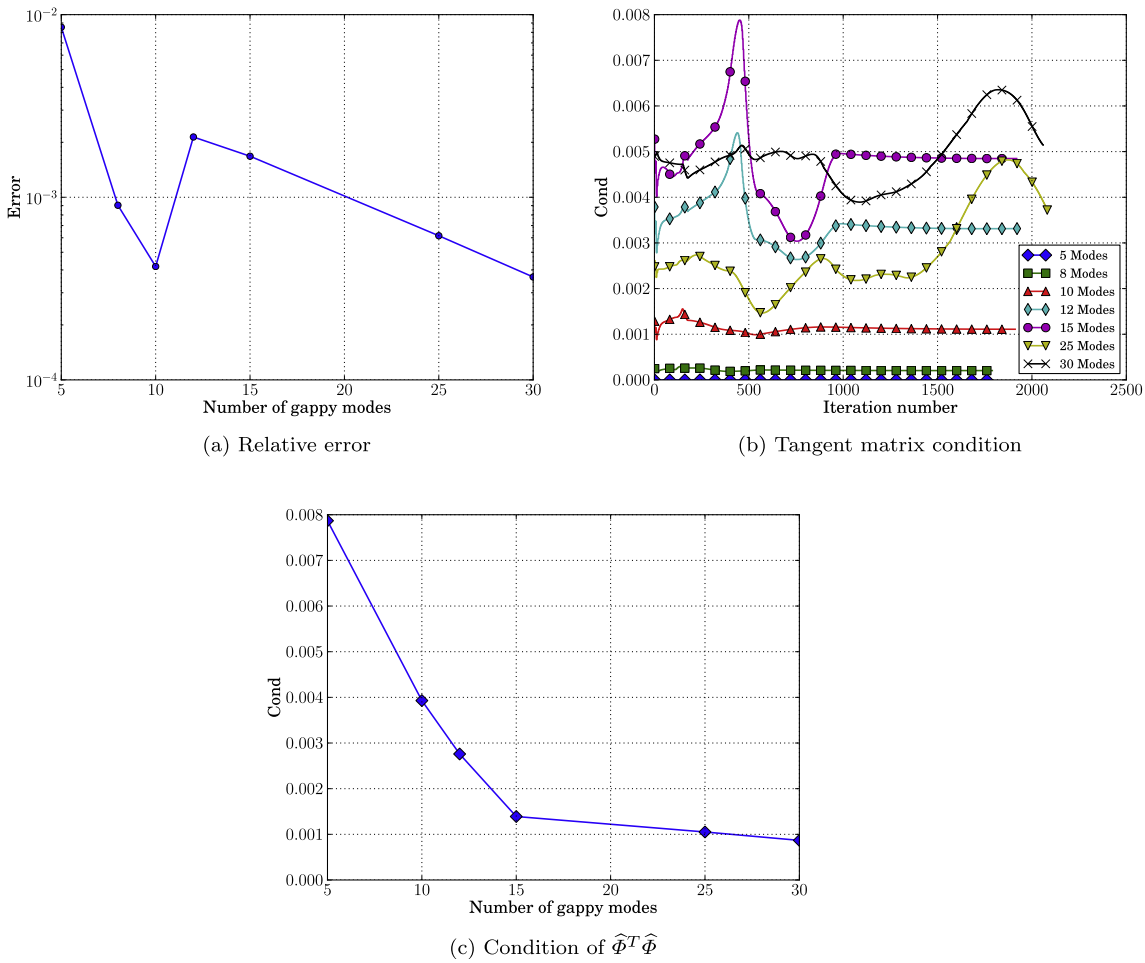

(a) Relative error

(b) Tangent matrix condition

(c) Condition of $\widehat{\Phi}^T\widehat{\Phi}$

Fig. 4. Solidifying cube problem: hyper-reduction of the residual. Results obtained by varying the number of gappy modes and sampling points with $k = 4$ and $n_s = n_g$.

Fig. 4 displays the results obtained using $k = 4$ projection modes, and a varying number of gappy modes n_g and sampling points n_s with $n_s = n_g$. Even with a large number of gappy modes, i.e., $n_g = 30$, the error of the approximation is always greater than 1×10^{-4} and therefore, the performance is not satisfactory. In this sense, the expectation of using a few sampling

points to obtain a good approximation to the residual is not met. Moreover, the condition numbers of the tangent matrix and of the matrix $\widehat{\Phi}^T\widehat{\Phi}$ are quite small, which affects the robustness of the HROM.

To improve the performance of this HROM, we double the number of gappy points, i.e., we run the tests using $k = 4$ and $n_s = 2n_g$. As observed in Fig. 5(a)–(c), better results are obtained but the condition numbers of the involved matrices are

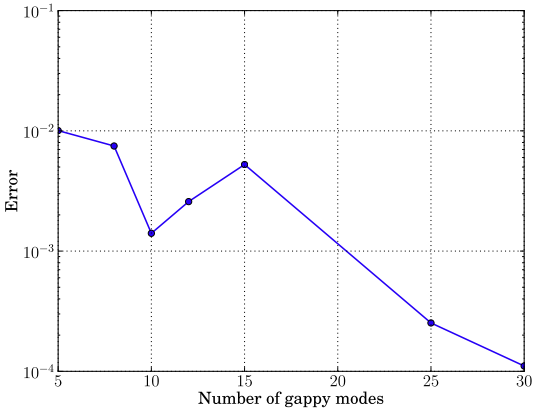

(a) Relative error

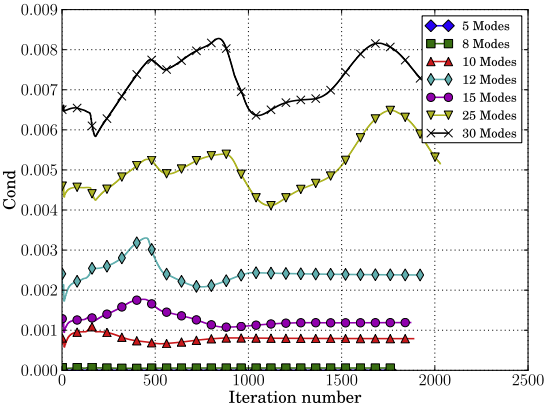

(b) Tangent matrix condition

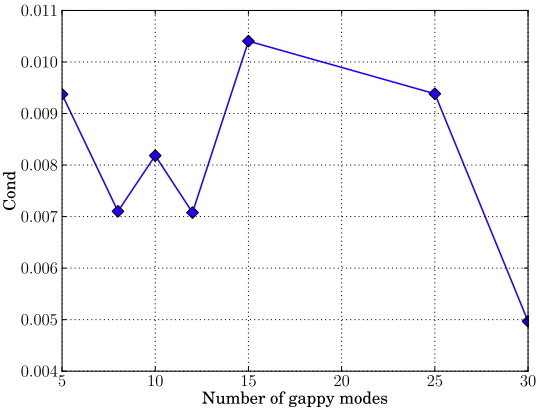

(c) Condition of $\widehat{\Phi}^T\widehat{\Phi}$

Fig. 5. Solidifying cube problem: hyper-reduction of the residual. Results obtained by varying the number of gappy modes and sampling points with $k = 4$ and $n_s = 2n_g$.

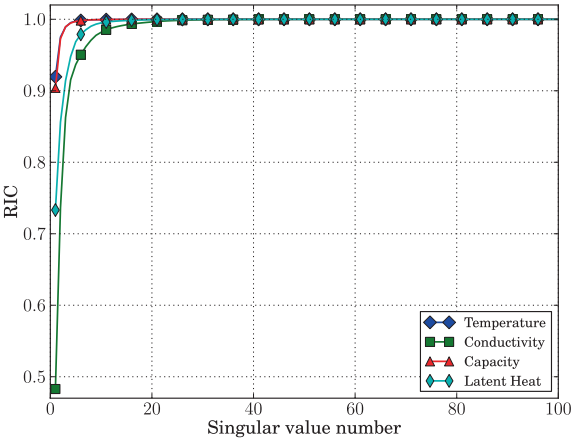

Fig. 6. Solidifying cube problem: hyper-reduction of separate contributions to the residual. SVD spectrum for each of the involved terms.

rather small, and the error reached is almost 1×10^{-4} when using 60 sampling points, which is much more than expected from the SVD spectrum.

Finally, a speedup test was run, using $k = 4$, $n_g = 30$ and $n_s = 60$ which corresponds to an error of 1.10×10^{-4} and produces a speedup of 74.9.

6.1.2. Results obtained by hyper-reducing the separate contributions to the residual

The cube solidification test is solved next using the HROM that separately hyper-reduces each contribution to the residual. Fig. 6 displays the SVD spectrum for each of the involved terms in the formulation. Again, a good HROM approximation is expected using a small number of sampling points, because the spectrum shows high compression. As shown in the following, this expectation is confirmed by the experiments.

Fig. 7 plots the results obtained using $k = 4$ projection modes, and a varying number of gappy modes n_g and sampling points n_s with $n_s = n_g$. By comparing these results with those presented in Fig. 4, we conclude that this HROM performs much better than the previous one, not only because the number of gappy points required to reach a given error is smaller, but also because the condition of the involved matrices is larger, thus contributing to the robustness of the method. Moreover, using $k = 4$ and $n_g = n_s = 5$, a relative error of 1.20×10^{-4} is obtained with a speedup of 336.25. When using $k = 4$ and $n_g = n_s = 12$, the relative error is 8.27×10^{-6} and the speedup is 224.9.

To further analyse the behaviour of this HROM, we run a test that augments the number of gappy points to $n_s = 2n_g$. The number of projection modes was held equal to $k = 4$, and the results can be observed in Fig. 8(c). The condition number of the involved matrices remain essentially unchanged. The computational error does not decrease significantly, making it necessary to increment the number of projection modes k if better results are required, e.g., by incrementing k to 8 and using $n_s = n_g = 12$, an error of 1.82×10^{-7} is obtained. We can conclude that in this case the error was governed by the number of projection modes and that the computation of the contributions to the residual were sufficiently accurate with $n_s = n_g$.

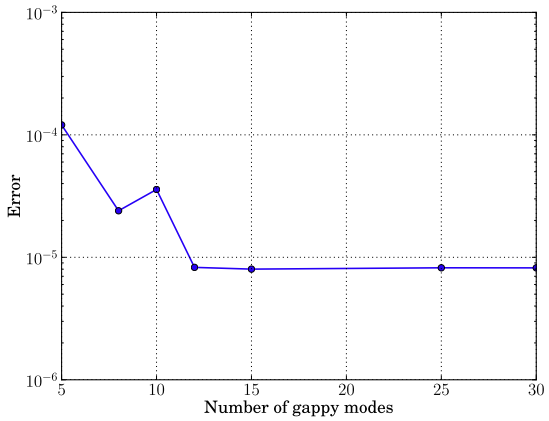

(a) Relative error

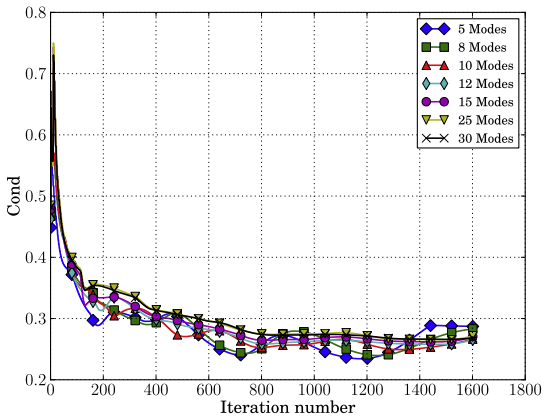

(b) Tangent matrix condition

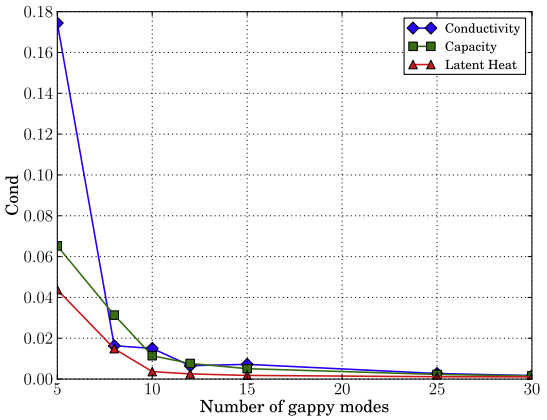

(c) Condition of $\widehat{\Phi}_i^T \widehat{\Phi}_i$

Fig. 7. Solidifying cube problem: hyper-reduction of separate contributions to the residual. Results obtained by varying the number of gappy modes and sampling points with $k = 4$ and $n_s = n_g$.

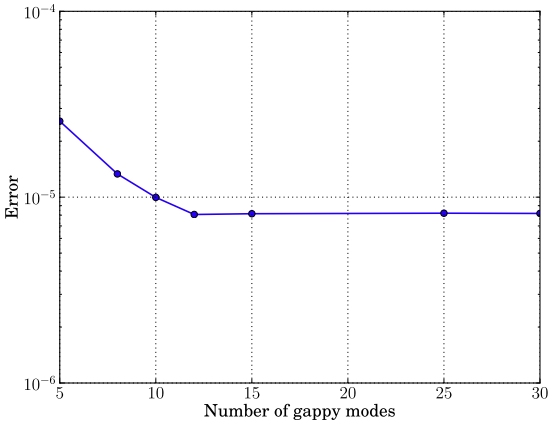

(a) Relative error

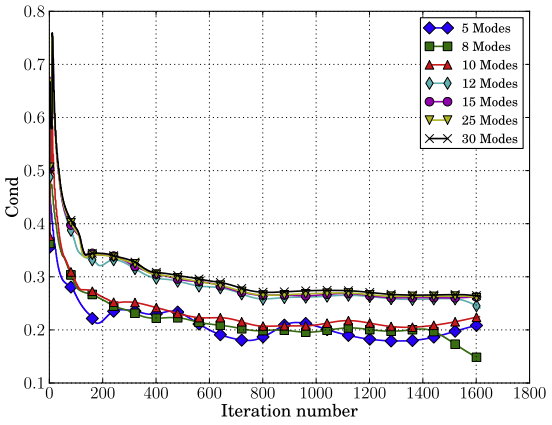

(b) Tangent matrix condition

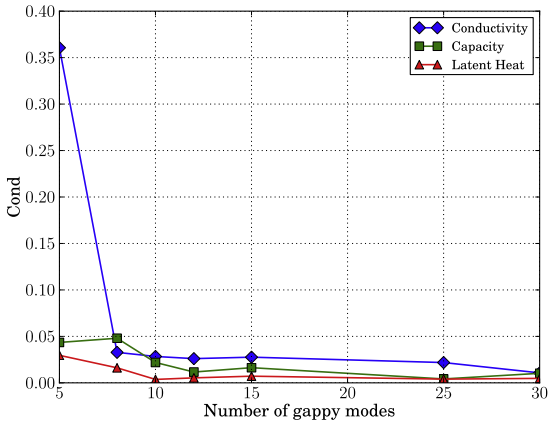

(c) Condition of $\widehat{\Phi}_i^T \widehat{\Phi}_i$

Fig. 8. Solidifying cube problem: hyper-reduction of separate contributions to the residual. Results obtained by varying the number of gappy modes and sampling points with $k = 4$ and $n_s = 2n_g$.

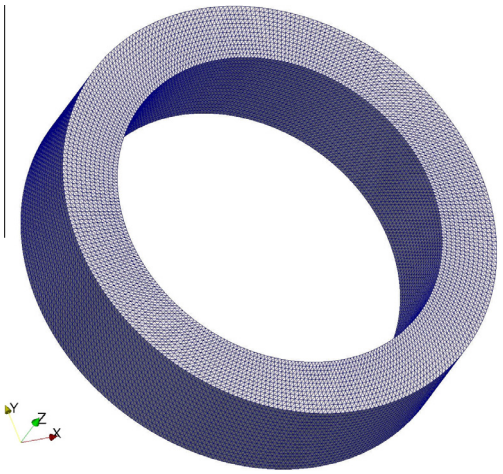

Fig. 9. Tube discretisation.

6.2. Welding of a tube

This problem consists of welding of a tube without material deposition. The external radius of the tube is 0.075 m and the internal radius is 0.05615 m. Symmetry conditions with respect to the x–y plane are applied, and only one half of the tube is modelled with a length of 0.0377 m. Robin boundary conditions are imposed at the internal and external surfaces. Fig. 9 shows the discretisation composed of 388800 tetrahedra and 74100 degrees of freedom. A time step of 0.15 s is used for the time interval $[0, 100]$ s. Temperature dependent thermophysical properties are used as specified in Fig. 10(b) and (a). The material density is $\rho = 4430 \frac{\text{kg}}{\text{m}}$, the solidus temperature is 1877 K, the liquidus temperature is 1933 K, and the latent heat is $\mathcal{L} = 292600 \frac{\text{J}}{\text{kg}}$. The heat source parameters are listed in Table 1. Initially, the heat source is located at the position given by the point $(-0.075, 0, 0)$. At the time instant $t = 0$, the heat source begins to travel with a constant tangential velocity equal to $5 \times 10^{-3} \frac{\text{m}}{\text{s}}$. The CPU time consumption required to obtain the HF solution was 11993.1 s. In the following, the reported speedups are obtained relative to this value.

6.2.1. Results obtained by hyper-reducing the residual

The welding problem is first solved by application of the HROM presented in Section 4.1 with a fixed reference frame. Fig. 11 presents the SVD spectrum of the temperature and the residual histories. It can be observed that the spectrum of

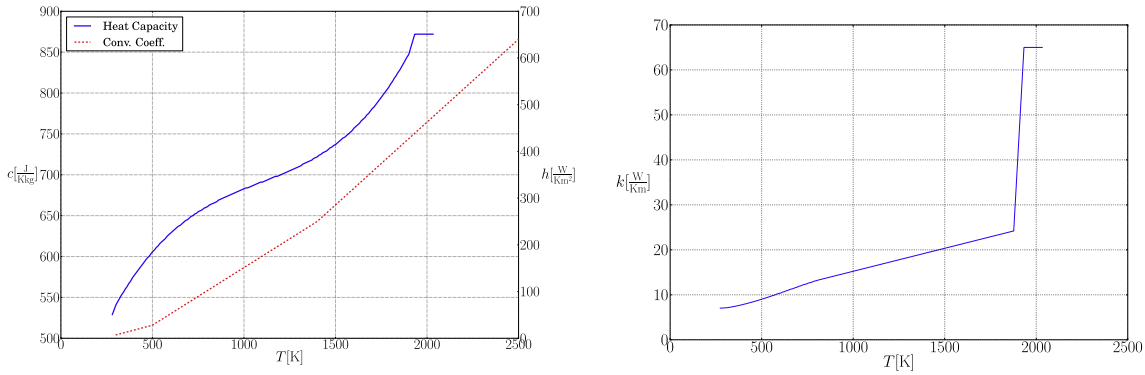

(a) Convection/radiation coefficient and heat capacity (b) Heat Conductivity

Fig. 10. Thermophysical properties.

Table 1
Parameters of the Goldak heat source.

a_r	a_f	b	c	f_f	I	V	η
10.84 mm	5 mm	5 mm	2 mm	0.63131	260 A	12 V	0.7

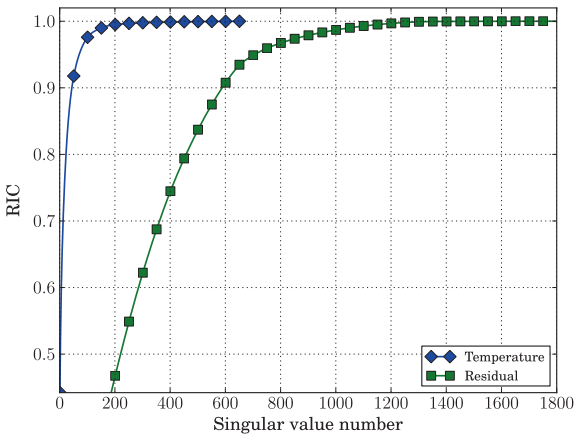

Fig. 11. Tube welding problem: hyper-reduction of the residual. SVD spectrum for each of the involved terms.

the residual is not as compact as the spectrum of the temperature, which is an indication of an inconvenience in the HROM, implying that a large number of sampling/gappy points must be used to build good approximations of the residual. Therefore, this HROM must use a large number of sampling points to capture the residual behaviour. For example, to obtain a relative error of 0.0010254, $k = 180$ projection modes, $n_g = 1200$ gappy modes and $n_s = 2400$ sampling points are required, thus affecting the performance (the speedup factor is only 18.06).

In this case, the condition number of $\widehat{\Phi}^T\widehat{\Phi}$ is 0.2919, although the situation is worse for the conditioning of the tangent matrix. For the iterations of the Newton–Raphson scheme, the average, the maximum and the minimum value of this condition number are given by 2.04×10^{-5}, 4.82×10^{-5} and 1.70×10^{-5}. In this context, even if the Newton–Raphson scheme converges, it cannot be guaranteed that a good approximation to the solution is obtained with the HROM. The bad performance and the ill-conditioning of the tangent matrix are related to the fact that the snapshots of the residual are zero everywhere except for a small region, where the residual's behaviour tends to be noisy (see, e.g., the residual corresponding to the first iteration at two different time steps in Fig. 12(a) and (b)).

6.2.2. Results obtained by hyper-reducing the separate contributions to the residual

The welding problem is solved next by the application of the HROM that separately hyper-reduces each contribution to the residual, with a fixed reference frame. Fig. 12(c) and (d) show the heat capacity contribution to the converged residual at two different time steps. The pattern is less noisy than the residual that was used to build the projection basis in the previous HROM. Therefore, the resulting SVD spectrum for each of the involved terms in the formulation is more compact than in the previous HROM, as shown in Fig. 13.

In an initial test, we selected a number of modes and sampling gappy points that were both equal to 200, i.e., $n_g = n_s = 200$, and analysed the variation of the relative error in terms of the selected number of projection modes k. Fig. 14(a) shows the evolution of this error. Initially, the error decreases when incrementing the number of projection modes but stagnates for $k > 120$. Fig. 14(b) gives an explanation for this phenomenon. First, the condition number of the tangent matrix decreases with the increment of the number of projection modes, indicating that the problem condition deteriorates and errors increase. Even worse, the condition numbers of the matrices associated with the gappy data reconstruction process are also quite low: $\text{cond}(\widehat{\Phi}_c^T\widehat{\Phi}_c) = 5.75 \times 10^{-5}$ and $\text{cond}(\widehat{\Phi}_k^T\widehat{\Phi}_k) = 0.007$. The error induced by the interpolation of the internal forces (gappy data reconstruction) is therefore quite large; it deteriorates the condition number of the tangent matrix, and the algorithm is not able to decrease the computation error when augmenting the number of projection modes.

The same experiment was performed but with the doubling of the number of sampling points: $n_g = 200$ and $n_s = 400$. The results can be observed in Fig. 15(a) and (b). The relative error of the solution is much smaller than before whereas the condition number of the tangent matrix increases with respect to the previous computation. In this case, the condition number of the matrices associated with the gappy procedure are $\text{cond}(\widehat{\Phi}_c^T\widehat{\Phi}_c) = 0.00104$ and $\text{cond}(\widehat{\Phi}_k^T\widehat{\Phi}_k) = 0.0686$, showing an increase of at least one order of magnitude with respect to the previous computation.

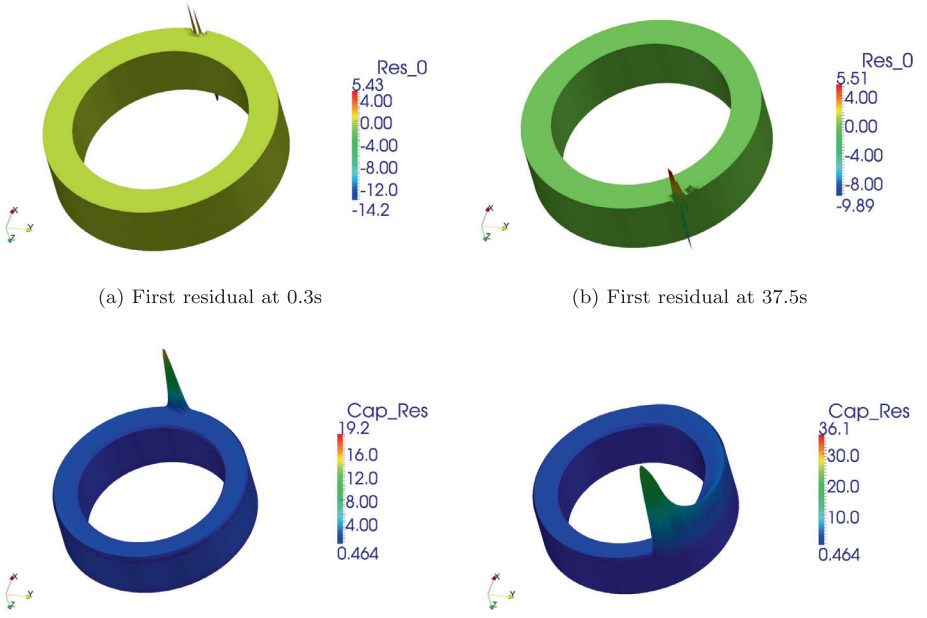

(a) First residual at 0.3s

(b) First residual at 37.5s

(c) Heat Capacity at 0.3s

(d) Heat Capacity at 37.5s

Fig. 12. Comparison of the quantities hyper-reduced by each of the introduced formulations. The visualisation used a deformation factor of 0.005 for wrapping the considered scalar quantities in the $-z$ direction.

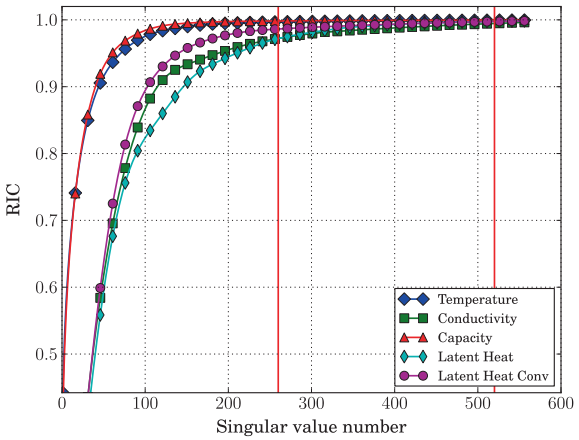

Fig. 13. Tube welding problem: hyper-reduction of the separate contributions to the residual. SVD spectrum for each of the involved terms.

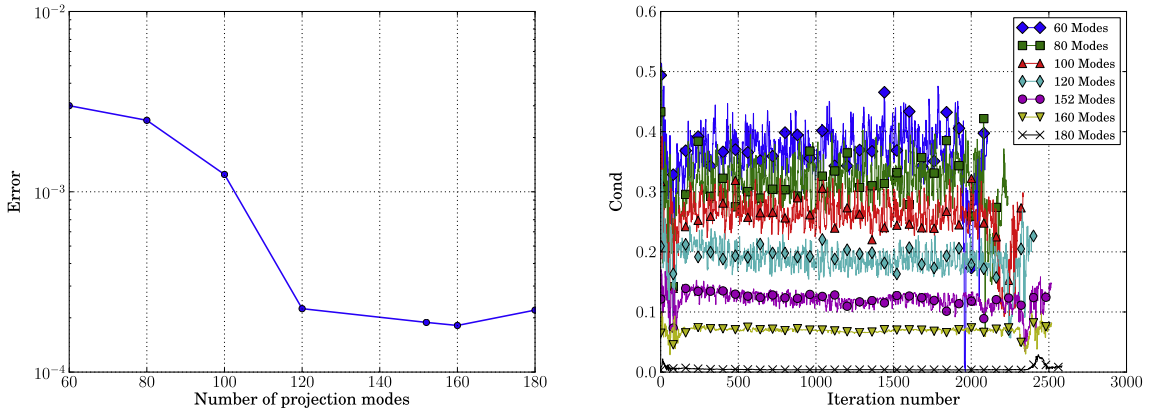

(a) Relative error for $n_g = 200$ and $n_s = 200$

(b) Tangent matrix condition

Fig. 14. Tube welding problem: hyper-reduction of the separate contributions to the residual. Results obtained by varying the number of projection modes for $n_g = 200$ and $n_s = 200$.

Next, we analyse how the HROM behaves when varying the number of modes and sampling points in the gappy data procedure. We leave the number of projection modes fixed at $k = 180$, and we progressively increment the number of gappy modes n_g and sampling points n_s while retaining the rule $n_s = 2n_g$. The results are shown in Fig. 16(c). In this case, the condition of the tangent matrix improves in response to an increment of the number of sampling points. However, the error of the approximation does not show any improvement because it is controlled by the number of projection modes.

To assess the computational performance, we measured the speedup using $n_g = 260$ and $n_s = 520$ (vertical lines in Fig. 13) for a varying number of projection modes. The result is shown in Fig. 17: the speedup decreases slightly when the number of projection modes is increased, attaining maximum and minimum values of 83.98 and 66.75, respectively.

6.2.3. Results obtained with the moving frame approach

Finally, the welding problem is solved by application of the HROM that separately hyper-reduces each contribution to the residual using a moving reference frame attached to the heat source. Fig. 18 shows the SVD spectrum for each term to be hyper-reduced. Comparing these spectra with those of Fig. 13, it can be expected that the performance of this model would be improved because these spectra are more compact than the previous spectra.

When 20 modes are used for the projection, a RIC of 99.7% is obtained; this indicator shows that the dynamics can be captured with a lower number of modes. Based on this plot, a number of $n_g = n_s = 35$ gappy modes and sampling points were used to interpolate the different contributions to the residual (see the vertical line in Fig. 18). Therefore, we analysed the variation of the relative error of the HROM in terms of the number of projection modes k from 1 to 20, holding $n_g = n_s = 35$. From the results shown in Fig. 19, it can be concluded that the HROM performs quite well with an acceptable condition number for the tangent matrix. The same can be said of the computational savings. The CPU time consumption for

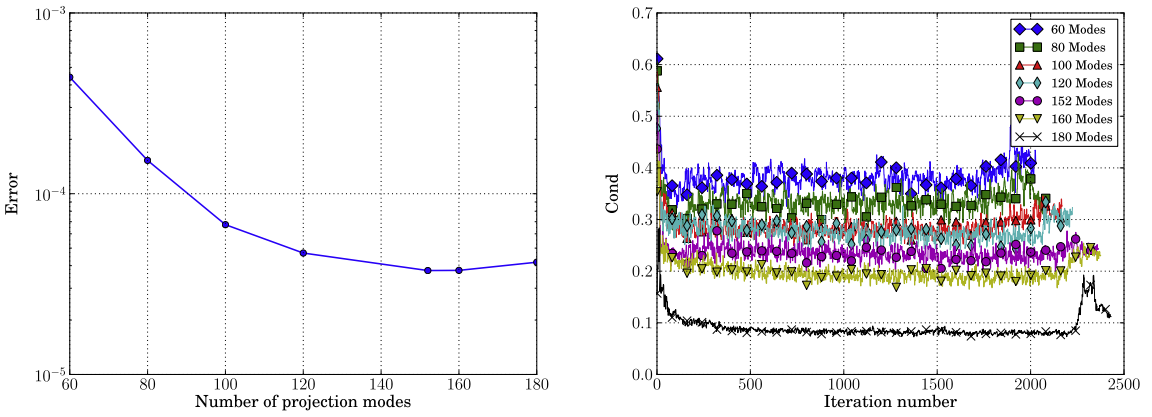

(a) Relative error for $n_g = 200$ and $n_s = 400$ (b) Tangent matrix condition

Fig. 15. Tube welding problem: hyper-reduction of the separate contributions to the residual. Results obtained by varying the number of projection modes for $n_g = 200$ and $n_s = 400$.

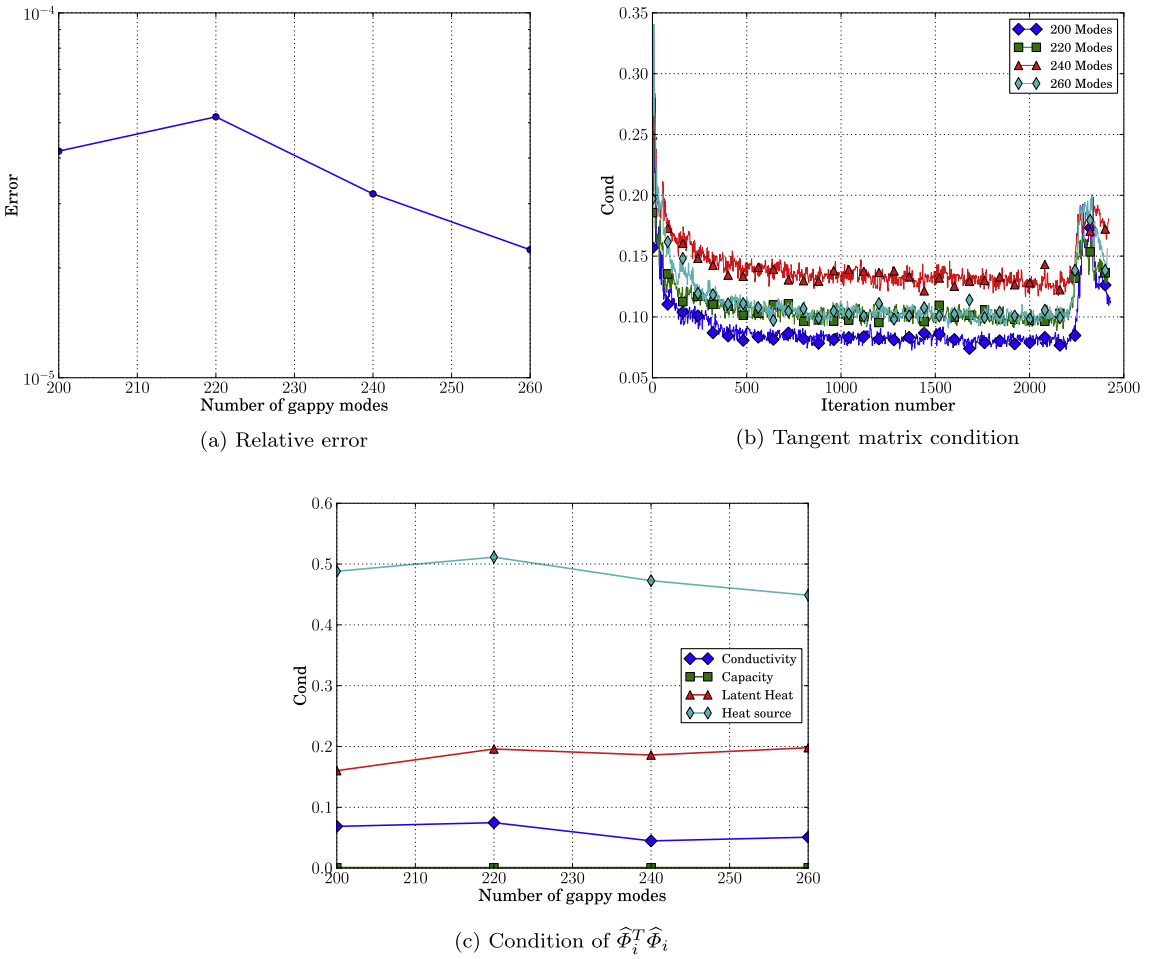

(a) Relative error (b) Tangent matrix condition

(c) Condition of $\widehat{\Phi}_i^T \widehat{\Phi}_i$

Fig. 16. Tube welding problem: hyper-reduction of the separate contributions to the residual. Results obtained by varying the number of gappy modes and sampling points with $k = 180$ and $n_s = 2n_g$.

the HF solution was 9817.4 s. Fig. 20 displays the variation of the speedup in terms of the number of projection modes k using $n_g = n_s = 35$. In this case the speedup attains a maximum value of 246.9. This speedup is higher than that obtained in the previous case, particularly because the number of gappy modes and sampling points is much lower than before.

To investigate the limits of this formulation, we studied how the increment in the number of gappy modes and sampling points affects the performance if the number of projection modes is fixed. Clearly, the computational performance will be affected because we are incrementing the number of sampling points. However, the objective is to evaluate what happens

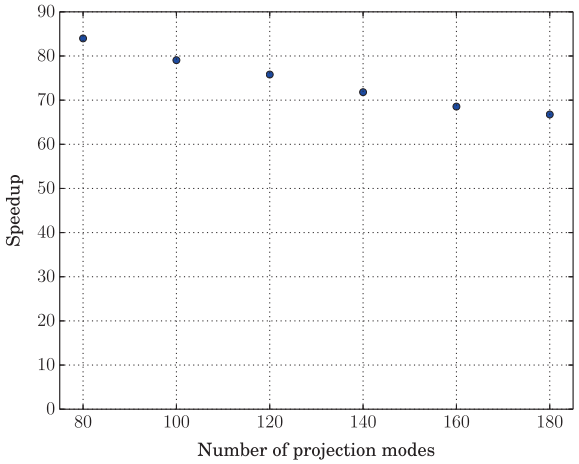

Fig. 17. Speedup.

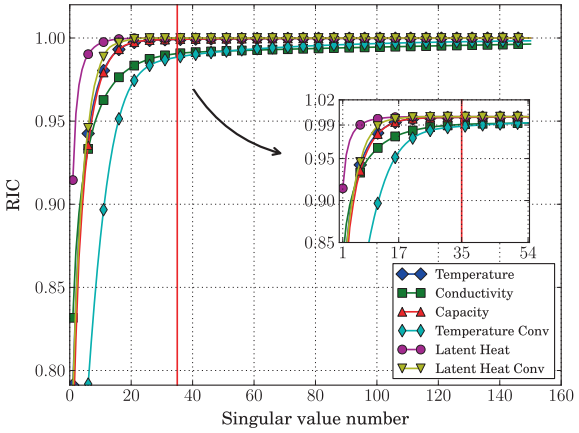

Fig. 18. Tube welding problem in a moving frame: hyper-reduction of the separate contributions to the residual. SVD spectrum for each of the involved terms.

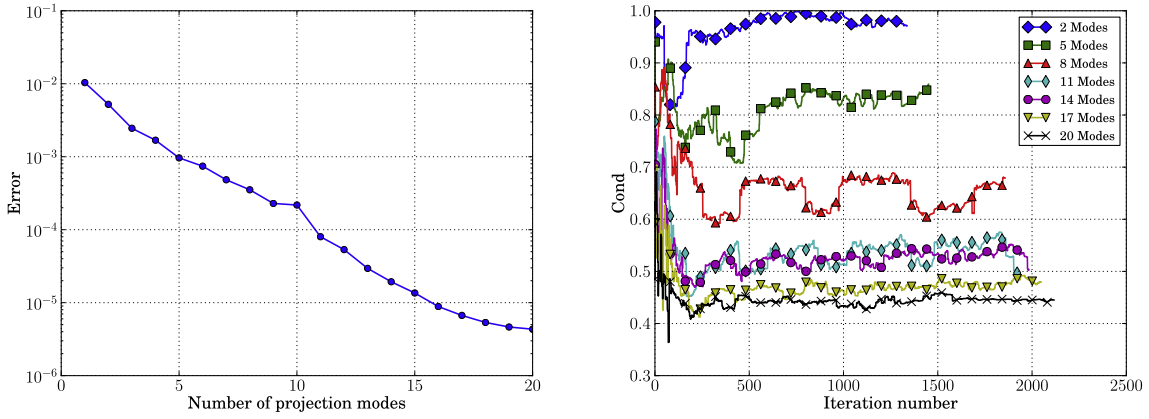

(a) Relative error for $n_g = n_s = 35$ (b) Tangent matrix condition

Fig. 19. Tube welding problem in a moving frame: hyper-reduction of the separate contributions to the residual. Results obtained by varying the number of projection modes for $n_g = n_s = 35$.

with the relative error and the condition of the tangent matrix when varying the number of modes and sampling points in the interpolation of the contributions to the residual.

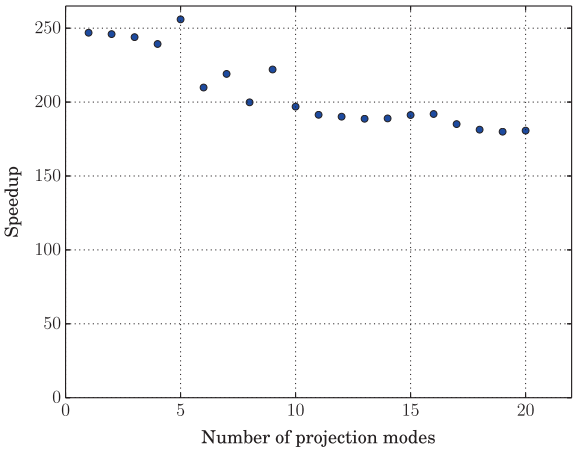

Fig. 20. Speedup in terms of the number of projection modes for $n_g = n_s = 35$.

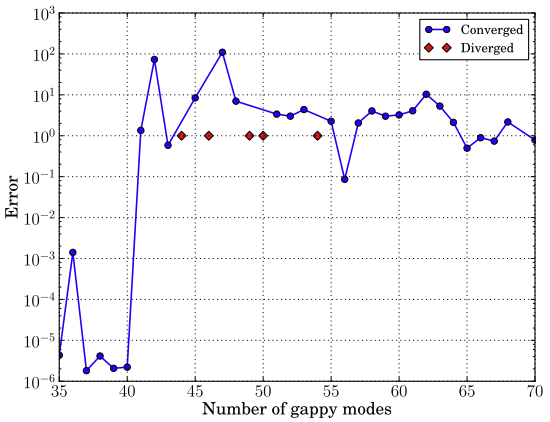

(a) Relative error

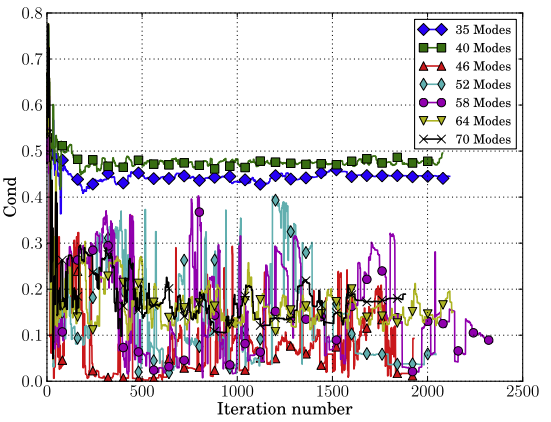

(b) Tangent matrix condition

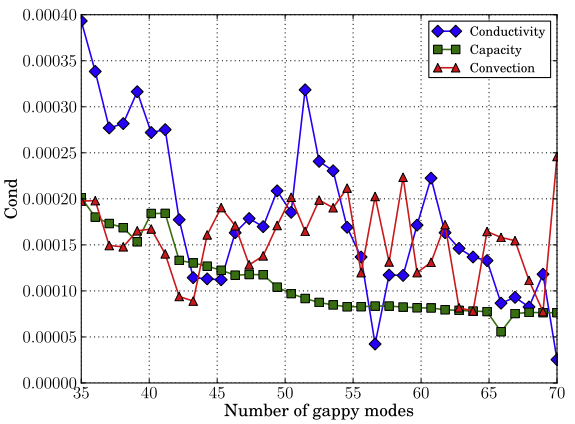

(c) Condition of $\widehat{\Phi}_i^T \widehat{\Phi}_i$

Fig. 21. Tube welding problem in a moving frame: hyper-reduction of the separate contributions to the residual. Results obtained by varying the number of gappy modes and sampling points with $k = 20$ and $n_g = n_s$.

Fig. 21(a) shows the variation of the relative error in terms of the number of gappy modes and sampling points ($n_g = n_s$) and always using $k = 20$ projection modes. It can be observed that for $n_g = n_s > 40$, the HROM solution displays a large error and does not converge in certain cases. This behaviour can be attributed to the fact that with the increment of the number of gappy modes, the condition of the tangent matrix and of the matrices cond($\widehat{\Phi}_i^T \widehat{\Phi}_i$) deteriorates, as shown in Fig. 21(b) and (c).

This situation is corrected using a greater number of sampling points, n_s, than gappy points, n_g. For instance, the number of sampling points is now selected as twice the number of gappy points ($n_s = 2n_g$). Fig. 22(a–c) show that for $n_g \geqslant 42$ and $k = 20$, the error decreases almost monotonically with the number of selected gappy, while the matrices conditioning is kept at reasonable values. The increment in the number of sampling points decreases the error of interpolation in the gappy procedure, and the condition of the resulting matrices improves. Note that the error was already quite low for $n_g = 40$ and that by adding additional points, only a small decrease in the error is produced because no significant information is added to the model.

Finally, for completeness, we present in Fig. 23 the location of the sampling points selected for the term $\boldsymbol{G}^k$ when using $n_g = n_s = 35$. We show that most of the sampling points are located notably close to the zone in which the high temperature gradients are produced, but several points are also almost uniformly distributed in the rest of the domain.

The previous tests were intended to draw the attention to the behaviour of each of the presented HROMs. Properties such as error, speedup, compressibility and conditioning were studied for each HROM, showing the ability of each one for reproducing the results of the HF training model. These did not consider parameters variation, that is, the problem solved by the HROM was the same as that used for training. For the present work this analysis suffices for pointing out the potential of each HROM, and more specifically for illustrating the different alternatives for ensuring the *compressibility* of the involved terms. Despite this fact, it would be interesting to study how parameters variation affect the performance, and more specifically the accuracy of the presented HROMs. It is not the purpose of this work to give a complete answer to this matter, but to give an insight by analysing the error obtained with the current HROM when a set of parameters different than those of the training problem are used.

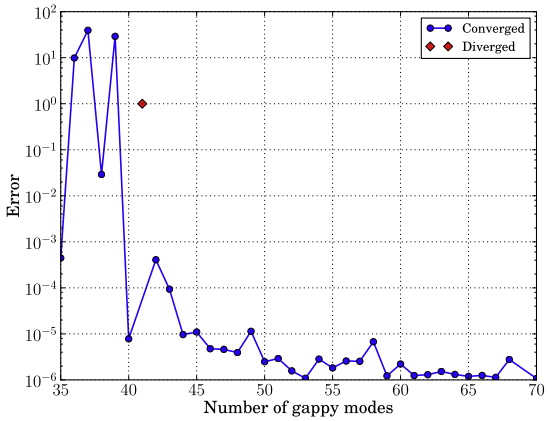

(a) Relative error

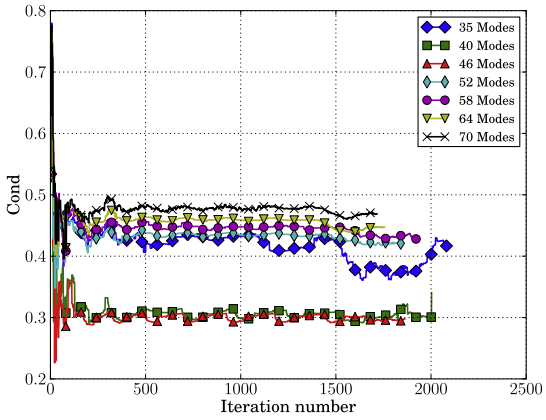

(b) Tangent matrix condition

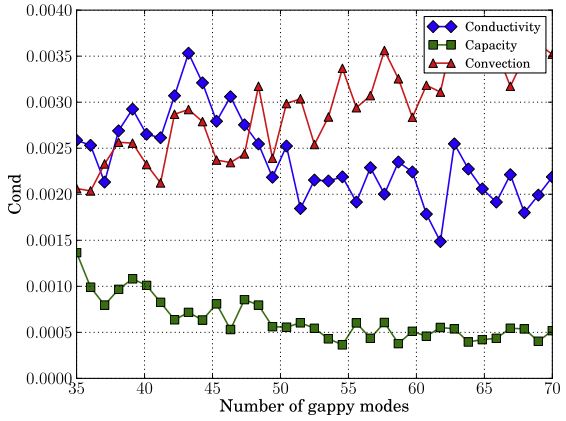

(c) Condition of $\widehat{\Phi}_i^T \widehat{\Phi}_i$

Fig. 22. Tube welding problem in a moving frame: hyper-reduction of the separate contributions to the residual. Results obtained by varying the number of gappy modes and sampling points with $k = 20$ and $n_s = 2n_g$.

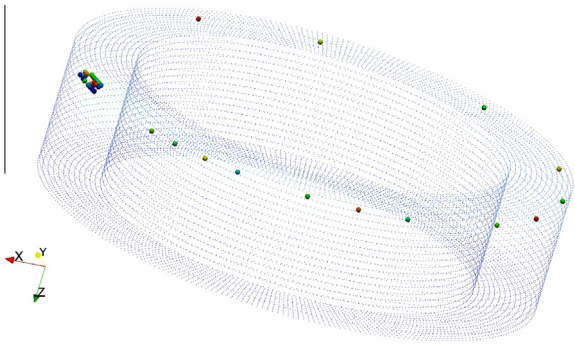

Fig. 23. Sampling points selected for the term $\boldsymbol{G}^k$ using $n_g = n_s = 35$.

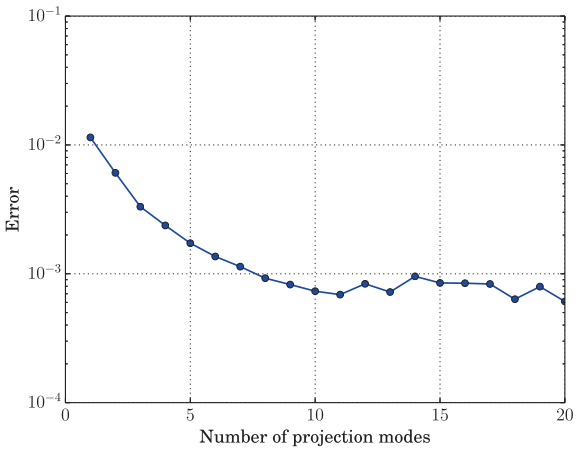

Fig. 24. Relative error for $n_g = n_s = 35$.

Specifically, a welding problem with the following characteristics is run:

- conductivity $k = 0.9k_r$,
- heat capacity $c = 0.9c_r$,
- heat source velocity $v = 0.9v_r$,
- heat source intensity $I = 0.9I_r$,

where the subscript r denotes the value of the considered property in the training problem. The other parameters that define the problem were the same as those of the training problem. The relative error obtained with the current HROM using $n_g = n_s = 35$ and varying the number of projection modes is shown in Fig. 24. As it can be observed in the figure, the error is quite acceptable even though no parameter sampling was accomplished for building the snapshots set other than those of the training problem itself. It is interesting to observe that when the number of projection modes is greater than 11, the error keeps almost constant and no improvement of results is obtained. That is, these extra modes are not contributing with significant information to the solution of this specific problem. Nevertheless, notice that when solving the training problem with the HROM, the error keeps decreasing for a number of projection modes greater than 11 (see Fig. 19(a)).

Remark. The last test shows that the current HROM has the ability to predict the solution to a problem different from the training problem. However, a more deep study about this topic is needed and left for a future work.

7. Conclusions

In this work, different strategies were analysed for building Hyper-Reduced Order Models to solve nonlinear thermal problems, with applications for welding modelling. The considered methods are classified within the *a posteriori* techniques and are based on the Proper Orthogonal Decomposition approach.

Several aspects were examined. First, the manner in which the hyper-reduction is performed was considered. Two different methods were analysed: the hyper-reduction of the residual as a whole and a new proposal based on the separate

hyper-reduction of the different terms contributing to the residual, in which the subdivision in terms is based on the physical characteristics of the problem. It was shown that the compressibility of the information was improved by the latter technique, allowing us to obtain good representations with a smaller number of gappy modes than with the former technique. As a result, faster computations could be performed, and the formulation also led to better conditioning of the nonlinear equations to be solved, thus improving the convergence properties.

A second aspect considered was the use of moving frames to simulate welding-like problems. A moving frame approach was applied in which the frame was attached to the concentrated heat source. The experiments showed that the moving frame approach increased the compressibility of the information with a further reduction in the number of modes required to obtain accurate approximations to the solution. Again, the conditioning of the problem was improved with better convergence properties.

The formulations are based on the choice of three parameters to obtain a Hyper-Reduced Order Model: (i) the number of projection modes, k; (ii) the number of gappy modes, n_g; and (iii) the number of sampling points, n_s. It was shown that these numbers must be selected such that $k \leqslant n_g \leqslant n_s$ to verify consistency. Several experiments were carried out to demonstrate the effect of varying these parameters. It was also demonstrated how these parameters must be chosen to avoid inconveniences produced by ill-conditioned equations.

Two three-dimensional nonlinear application examples were extensively covered: a solidifying cube and a welding-like problem in which a concentrated heat source travels to simulate a welding torch. Speedups of up to 250 times with respect to the high fidelity solutions were observed in these examples showing the potential of the proposed techniques.

Future work will be carried out to further study the ill conditioning of the matrices involved in the HROM formulation and to find a method that can detect and avoid problems in the computations. Additionally, the hyper-reduction of welding problems with material deposition will be analysed together with an analysis of the range of validity of the HROMs under variations of the parameters that define the problem.

Acknowledgments

This work received financial support from Consejo Nacional de Investigaciones Científicas y Técnicas (CONICET), Universidad Nacional del Litoral (UNL), Autoridad Regulatoria Nuclear (ARN) and the European Research Council under the Advanced Grant: ERC-2009-AdG "Real Time Computational Mechanics Techniques for Multi-Fluid Problems".

References

[1] J. Ronda, G. Oliver, Consistent thermo-mechano-metallurgical model of welded steel with unified approach to derivation of phase evolution laws and transformation-induced plasticity, Comput. Methods Appl. Mech. Eng. 189 (2) (2000) 361–418, http://dx.doi.org/10.1016/S0045-782(99)00461-2.
[2] A. Anca, A. Cardona, J. Risso, V. Fachinotti, Finite element modeling of welding processes, Appl. Math. Model. 35 (2) (2011) 688–707.
[3] A. Nouy, A priori model reduction through proper generalized decomposition for solving time-dependent partial differential equations, Comput. Methods Appl. Mech. Eng. 199 (23–24) (2010) 1603–1626, http://dx.doi.org/10.1016/j.cma.2010.01.009.
[4] K. Kunisch, S. Volkwein, Galerkin proper orthogonal decomposition methods for a general equation in fluid dynamics, SIAM J. Numer. Anal. 40 (2) (2002) 492–515, http://dx.doi.org/10.1137/S0036142900382612.
[5] M. Bergmann, C.-H. Bruneau, A. Iollo, Enablers for robust POD models, J. Comput. Phys. 228 (2) (2009) 516–538, http://dx.doi.org/10.1016/j.jcp.2008.09.024.
[6] D. Ryckelynck, An a priori model reduction method for thermomechanical problems [Réduction a priori de modèles thermomécaniques], C.R. - Mec. 330 (7) (2002) 499–505.
[7] D. Néron, P. Ladevèze, Proper generalized decomposition for multiscale and multiphysics problems, Arch. Comput. Methods Eng. 17 (4) (2010) 351–372.
[8] F. Chinesta, A. Ammar, E. Cueto, Recent advances and new challenges in the use of the proper generalized decomposition for solving multidimensional models, Arch. Comput. Methods Eng. 17 (4) (2010) 327–350, http://dx.doi.org/10.1007/s11831-010-9049-y.
[9] E.J. Candes, T. Tao. Near-Optimal Signal Recovery From Random Projections: Universal Encoding Strategies? in: IEEE Transactions on Information Theory, vol. 52, 2006, pp. 5406-5425, http://dx.doi.org/10.1109/TIT.2006.885507.
[10] Y. Eldar, G. Kutyniok, Compressed Sensing: Theory and Applications, Cambridge University Press, 2012.
[11] K. Carlberg, C. Bou-Mosleh, C. Farhat, Efficient non-linear model reduction via a least-squares Petrov–Galerkin projection and compressive tensor approximations, Int. J. Numer. Methods Eng. 86 (2) (2011) 155–181, http://dx.doi.org/10.1002/nme.3050.
[12] A. Cardona, S. Idelsohn, Solution of non-linear thermal transient problems by a reduction method, Int. J. Numer. Methods Eng. 23 (6) (1986) 1023–1042, http://dx.doi.org/10.1002/nme.1620230604. <http://dx.doi.org/10.1002/nme.1620230604>.
[13] J. Hernández, J. Oliver, A. Huespe, M. Caicedo, High-performance model reduction techniques in computational multiscale homogenization, Comput. Methods Appl. Mech. Eng., submitted for publication.
[14] K. Carlberg, C. Farhat, J. Cortial, D. Amsallem, The GNAT method for nonlinear model reduction: effective implementation and application to computational fluid dynamics and turbulent flows, J. Comput. Phys. 242 (2013) 623–647.
[15] J. Baiges, R. Codina, S. Idelsohn, Explicit reduced-order models for the stabilized finite element approximation of the incompressible Navier–Stokes equations, Int. J. Numer. Methods Fluids 72 (12) (2013) 1219–1243, http://dx.doi.org/10.1002/fld.3777.
[16] S. Chaturantabut, D. Sorensen, Discrete empirical interpolation for nonlinear model reduction, in: Proceedings of the 48th IEEE Conference on Decision and Control, 2009 held jointly with the 2009 28th Chinese Control Conference, CDC/CCC 2009, 2009, pp. 4316–4321, http://dx.doi.org/10.1109/CDC.2009.5400045.
[17] D. Ryckelynck, A priori hyperreduction method: an adaptive approach, Journal of Computational Physics 202 (1) (2005) 346–366, http://dx.doi.org/10.1016/j.jcp.2004.07.015.
[18] B. Sarbandi, S. Cartel, J. Besson, D. Ryckelynck, Truncated integration for simultaneous simulation of sintering using a separated representation, Arch. Comput. Methods Eng. 17 (4) (2010) 455–463.
[19] R. Everson, L. Sirovich, Karhunen–Loeve procedure for gappy data, J. Opt. Soc. Am. A 12 (1995) 1657–1664.
[20] P. Astrid, Reduction of process simulation models: a proper orthogonal decomposition approach (Ph.D. thesis), Technische Universiteit Eindhoven, 2004.
[21] D. Ryckelynck, Hyper-reduction of mechanical models involving internal variables, Int. J. Numer. Methods Eng. 77 (1) (2009) 75–89.

[22] J. Goldak, A. Chakravarti, M. Bibby, A new finite element model for welding heat sources, Metall. Mater. Trans. B 15 (1984) 299–305.
[23] V.D. Fachinotti, A. Cardona, A.E. Huespe, A fast convergent and accurate temperature model for phase-change heat conduction, Int. J. Numer. Methods Eng. 44 (12) (1999) 1863–1884.
[24] A. Cosimo, V. Fachinotti, A. Cardona, An enrichment scheme for solidification problems, Comput. Mech. 52 (2013) 17–35.
[25] D. González, A. Ammar, F. Chinesta, E. Cueto, Recent advances on the use of separated representations, Int. J. Numer. Methods Eng. 81 (5) (2010) 637–659 (Cited by (since 1996)25).
[26] I. Jolliffe, Principal Component Analysis, Springer Series in Statistics, Springer, 2002.
[27] L. Sirovich, Turbulence and the dynamics of coherent structures. I – Coherent structures. II – Symmetries and transformations. III – Dynamics and scaling, Q. Appl. Math. 45 (1987) 561–571.
[28] G. Strang, The fundamental theorem of linear algebra, Am. Math. Mon. 100 (9) (1993) 848–855.
[29] P. Wriggers, Nonlinear Finite Element Methods, Springer, Berlin, 2008.
[30] C.T. Kelley, Iterative Methods for Optimization, Society for Industrial and Applied Mathematics, Philadelphia, 1999.
[31] D. Galbally, K. Fidkowski, K. Willcox, O. Ghattas, Non-linear model reduction for uncertainty quantification in large-scale inverse problems, Int. J. Numer. Methods Eng. 81 (12) (2010) 1581–1608.
[32] N.C. Nguyen, J. Peraire, An efficient reduced-order modeling approach for non-linear parametrized partial differential equations, Int. J. Numer. Methods Eng. 76 (2008) 27–55, http://dx.doi.org/10.1002/nme.2309.
[33] G. Golub, C. Van Loan, Matrix Computations, Johns Hopkins Studies in the Mathematical Sciences, Johns Hopkins University Press, 1996.
[34] N.C. Nguyen, A.T. Patera, J. Peraire, A 'best points' interpolation method for efficient approximation of parametrized functions, Int. J. Numer. Methods Eng. 73 (4) (2008) 521–543, http://dx.doi.org/10.1002/nme.2086.
[35] M. Barrault, Y. Maday, N.C. Nguyen, A.T. Patera, An 'empirical interpolation' method: application to efficient reduced-basis discretization of partial differential equations, C.R. Math. 339 (9) (2004) 667–672, http://dx.doi.org/10.1016/j.crma.2004.08.006.